21333-6020-RU-00

FINAL REPORT

STUDY OF RELATION BETWEEN Pc 3 MICROPULSATIONS AND MAGNETOSHEATH FLUCTUATIONS, AND MULTISATELLITE INVESTIGATION OF EARTH'S BOW SHOCK

30 August 1975

Prepared for
National Aeronautics and Space Administration
Washington, D.C.

Contract No. NASW-2398

by

Eugene W. Greenstadt

Space Sciences Department
TRW Systems
One Space Park
Redondo Beach, California 90278

TABLE OF CONTENTS

INTRODUCTION

This report summarizes the approaches, procedures, and results obtained by this study during the year 1 September 1974 - 31 August 1975. Ensuing sections review the Background, Objectives, Results, and Reports of the past year's efforts. The document closes with Commentary and Recommendations sections. As usual, the main body of the report is short, and technical details of the new results are elaborated in the Appendices, which are preprints or drafts of papers submitted, or in late stages of preparation, for publication. One result described in a preprint attached to the semi-annual report and another attached to the proposal for continuation are not repeated as appendices here, for reasons of economy.

BACKGROUND

Purpose. The existing program (NASW-2398) has had basically a twofold purpose. First, to test the valididity of a suggested model according to which Pc 3 and/or Pc 4 micropulsations are excited by magnetosheath field (and plasma) fluctuations arising in the quasi-parallel structure of the subsolar bow shock; second to expand and deepen our understanding of the influence of solar wind plasma parameters on local shock structure and on the configuration of the entire bow shock system.

Micropulsations. Certain micropulsations, especially Pc 3 (period range 10-45 sec), have shown strong correlation of their various characteristics with solar wind features. These correlations, together with the results on field-dependent shock and sheath structure obtained by the present investigator, led to his suggesting a mechanism whereby the interplanetary field $\underset{\sim}{B}_{SW}$ should strongly influence the excitation of Pc 3 at the magnetopause when it

aligns itself with solar wind velocity $\underset{\sim}{V}_{SW}$, thus causing large amplitude waves at the subsolar point of the shock. The waves should be conveyed to the magnetopause by the pattern of solar wind flow in the magnetosheath. Additional factors expected to contribute to the postulated model are thermal-to-field energy ratio β, solar wind mach number M, and the state of the magnetosphere.

Shock Structure. Collisionless plasma shock structure is determined in all scale lengths by the three plasma parameters, or, more precisely, the three classes of plasma parameters β, M, and θ_{nB}, denoting the thermal-to-field energy ratio, mach number, and field-to-shock normal angle, respectively (Tidman and Krall, 1971). We say classes of parameters because different constituents of the plasma may have different β's and different wavemodes may have separate M's, some dependent in turn on θ_{nB}. A full description of shock-structural processes can be arrived at with multiple satellite measurements only if the effect of each of the relevant parameters can be isolated.

This study has emphasized the use of simultaneous data from two or more spacecraft and from multiple diagnostics to evaluate the geometrical factor θ_{nB}, or, more precisely in some cases, its B-X equivalent, and the principal plasma parameters. More recently, attention has been divided between large scale characterization of the bow shock system, including upstream and downstream perturbations, and fine scale comparison between observed shock features and plasma theoretical predictions.

OBJECTIVES

At the beginning of this year's work, a computer program was completed at TRW for producing plots of θ_{XB} on arbitrary time scales from Explorer 35 magnetic field tapes. Later, a program was finished at the University of Alberta for generating spectrograms of micropulsations in the Pc 3-4 period range, with the aim of testing objectively the correlation reported by other researchers. Copies of the θ_{XB} graphs were also sent to UCLA, College and Sendai, where micropulsation observers had expressed interest in aiding this study. The second half of this year's work was to focus on comparisons of θ_{XB} with various versions of Calgary magnetograms.

The investigation of bow shock structure was to be pursued along any or all of several avenues. These were:

1. Comparison of shock profiles for different solar wind parameter values;

2. Study of specific cases in detail at high resolution;

3. Estimation of effective resistivity in the very well documented laminar shock crossings of 12 February 1969;

4. Examination of the phenomenology of proton reflection from the shock and of upstream wave generation.

RESULTS

Micropulsations

The creation of compatible records of θ_{XB} and Pc 3,4 amplitude behavior proved long and arduous. Digital spectrograms and, later, filtered ampligrams were finally made which displayed micropulsation activity on various time scales as recorded at the Calgary observatory during part of the interval of interest in 1969.

The spectrally more complete, but visually more confusing, digital sonograms yielded a great deal of ambiguity in the sense that patterns of pulsation activity were scattered; θ_{XB} was often at "middle" values close to neither 0° nor 90°; there were numerous data gaps during "prime time" (i.e., local midday at Calgary); and θ_{XB} tended to vary rapidly within the unpromising middle of its range. A few sections of the record were found in which θ_{XB} took on, or switched between, sufficiently extreme values held for a sufficiently long time to support a first-order comparison with surface activity. These sections tended to support a positive correlation between low θ_{XB} and very high Pc 4 (but not Pc 3), activity. A description of these sections was given in the semiannual report of 31 March 1975. Since then, filtered ampligrams of the Pc 4 band have been run (Calgary data) and an initial comparison made of the output with θ_{XB}. The results are tentatively far from clearly supportive of the correlation proposed by this investigator's model and claimed by other observers.

Recently, the investigators enjoyed this first face-to-face meeting since the collaboration began, when John Olson (Edmonton) visited TRW with some fresh data runs. It was agreed that while some sections of the record

gave the impression of positive correlation too consistent for coincidence, other sections were decidedly incompatible with the model under study. However, there appeared to be a format-dependent effect with considerable potential significance to both the study technique and the physical process under examination. The filtered ampligrams present a rectified version of the signal passband, with the version run by Olson including the Pc 4 and Pc 5 bands. Rectification, or at least its plotted output, which involves squaring the original signal, tends to obscure the micropulsation baseline and to exaggerate transient effects in the Pc 5 band. The rectified Pc 5 ampligrams suggested a correlation between amplitude "pulses" and changes in θ_{XB}. A short section of filtered but unrectified signal brought by Olson as a sample just for visual calibration of the ampligrams gave a quite different impression of the micropulsation activity and was more supportive of the original correlation sought, but inconclusive because of its brevity. At this stage it may be speculated that pulses in the ampligram are representative of transient Pi 1 or Pi 2 rather than Pc 4 activity and these phenomena may correlate with directional variability of $\underset{\sim}{B}_{SW}$ instead of direction itself.

It was decided to run unrectified as well as rectified versions of the passband-filtered micropulsation for selected days of reasonably complete data, and these will be the basis for the next stage of comparison with θ_{XB}.

Shock Structure

General. A catalogue of observed shock structures for the common range of solar wind parameters M, β, θ_{nB} was drafted by Formisano last year, but

completion of the catalogue has been delayed for substantial revision of the figures (by Russell) and updating of the text (by Greenstadt). Meanwhile an interim review of experimental results on the bow shock was undertaken in response to an invitation to lecture at the Summer Advanced Study School in Graz. A report prepared on this topic, attached as Appendix A, is an expanded version of a shorter paper to be published in the Proceedings. Preparation of the review furnished an opportunity to contemplate some unexplained results, so the paper contained some suggested resolutions and some attempts to unify diverse, separately observed phenomena.

Case Studies. An example of bow shock profile with nearly parallel geometry was examined in detail. A draft report is attached as Appendix B. Submission of the report for publication is awaiting comments and corrections by all the coauthors.

A study of a shock crossing of unusually high Alfvén Mach number ($M_A \gtrsim 12$) was initiated. The electric plasma wave noise was extraordinarily high and extensive in this case.

Resistivity. Simple fluid approximations and an ion-acoustic model of resistive shock dissipation have been applied to the laminar crossings of 12 February 1969. The abstract of an oral presentation to the AGU was included with the Semiannual Report. A draft paper on one result has been prepared and is attached as Appendix C. The principal result of this first, brief study is that the shock thicknesses of main magnetic gradients in the cases examined are compatible with the maintenance of conditions of critical stability/instability for plasma wave heating of electrons alone.

Another approach to the same data, in which a two-fluid model is programmed to produce machine plots of oblique shock profiles matching those observed, has achieved its first real success during preparation of this annual report. The relative amplitude and damping rate of theoretical and measured upstream standing whistler waves have been matched by assuming pure resistive dissipation in the shock ramp, again with $\nu_{eff} \approx \omega_{pi}$. The result is shown in Figure 1. Note that the comparison in this figure is improved over that shown in the proposal submitted for continuation of the present study; in the earlier example the model didn't provide sufficient damping of the standing waves.

Reflected ions. A study of the forward boundary of upstream proton waves was completed, with the finding that the boundary behaved statistically as if protons were reflected from the bow shock with guiding center velocities 1.6 V_{SW} near the subsolar point and > 2 V_{SW} along the dayside flank. On the average, the reflection speed along the interplanetary field was $\approx 2\ V_{SW}$. A report has been accepted by JGR and was included with the proposal for continuation.

REPORTS

The following reports were prepared or published during the year.

Papers 1. Structure of the Quasi-Parallel, Quasi-Laminar Bow Shock, E. W. Greenstadt, C. T. Russell, V. Formisano, P. C. Hedgecock, F. L. Scarf, M. Neugebauer, and R. E. Holzer.

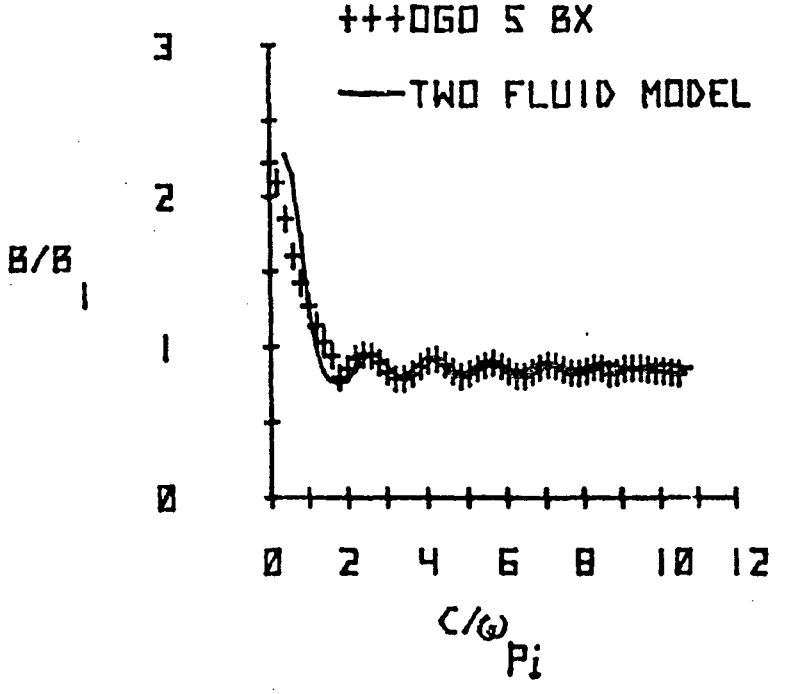

Figure 1. Comparison between observed and computed laminar shock profiles. The computed version assumes an effective collision frequency $\nu_{eff} \simeq \omega_{pi}$ in the shock ramp. The long ramp and sharp first-wave minimum of the observed profile were probably caused by shock motion.

2. Collisionless Shock Waves in Space: A Very High β Structure, V. Formisano, C. T. Russell, J. D. Means, E. W. Greenstadt, F. L. Scarf, and M. Neugebauer, J. Geophys. Res., 80, 2013, 1975.

3. A Statistical Study of the Upstream Wave Boundary Outside the Earth's Bow Shock, L. Diodato, E. W. Greenstadt, G. Moreno, and V. Formisano, submitted to J. Geophys. Res, in press.

4. Structure of the Quasi-Perpendicular, Laminar Bow Shock, E. W. Greenstadt, C. T. Russell, F. L. Scarf, V. Formisano, and M. Neugebauer, J. Geophys. Res., 80, 502, 1975.

5. Phenomenology of the Earth's Bow Shock System. A Summary Description of Experimental Results, E. W. Greenstadt, submitted for Proc. of Summer Advanced Study Institute, Graz, Austria, August 1975.

6. Thickness of Magnetic Structures Associated with the Earth's Bow Shock, D. L. Morse and E. W. Greenstadt, to be submitted to J. Geophys. Res. (also presented orally at June AGU Meeting, Washington, D.C.).

COMMENTARY

Concurrent research efforts by other workers in space physics have continued to produce results and ideas related to the objectives and results of this study. Theoretical treatments of the processes by which waves might interact with the magnetopause and penetrate the magnetosphere have been undertaken (Rajaram et al., 1974) and also compared with satellite spectral observations (Wolfe and Kauffman, 1975). Such investigations are of obvious importance to this study, which aims ultimately at demonstrating (or disproving) the thesis that waves of shock-structural origin are delivered to the magnetopause and excite micropulsations. In addition, this investigator found, on attendance at the Magnetospheric-Particles and Fields Conference in Graz, that certain areas of the magnetopause and mantle are being envisioned, at

least by some analysts (e.g., Haerendel), as composed of fairly intricate physical substructures with time constants comparable to the periodicities of shock and magnetosheath pulsations. Problems of relationship between these shock and magnetopause structures will ultimately come under scrutiny as experimental data and analytic techniques continue to improve.

The fundamental nature of the field-dependent shock structure in which this study has pioneered has been verified in the most gratifying way by recent data from Mercury and Jupiter flybys showing that the interaction regions of every planet from Mercury to Jupiter behave according to the pattern outlined by this investigator. Planetary magnetospheric encounters are now treated routinely by including shock-structural considerations in early analysis of the data.

RECOMMENDATION

Micropulsations. The attempted correlation of θ_{nB} with Pc 4 has reached a stage in which satisfactory documentation of the comparison between surface activity at Calgary and θ_{nB} variation at Explorer 35 is, or is on the verge of being, available. It is already clear that the correlation predicted by this investigator and, presumably, demonstrated by others is far from self-evident in the data set under study. Since it is also already clear that total contradiction is not evident, ambiguity is destined to be the initial result. We do not necessarily regard this as a setback, but rather as a guidepost along a path whose course is determined in a complicated way by several factors. It is recommended, and intended by the investigators, that the ambiguous result be documented and quickly reported in a short publication.

It is our hope that exposure of this outcome will stimulate wider interest and also provoke an exchange in which thorough discussion of both physical factors and experimental techniques will occur. As noted in previous reports of this study, details of the experimental and/or analytical methods employed by other workers, particular the Russians, have been sketchy at best, although their statistical or synoptic outcomes have appeared quite convincing. Cross-comparison may achieve a significant advance in our understanding of Pc 3, 4 phenomena.

Shock Structure. Numerous extensions of the empirical, multiple satellite data technique to cases and parameter sets still undocumented or unexplored can, and should, be carried out whenever the opportunity is presented. However, it is recommended that increased attention, and higher priority, be devoted to quantitative comparisons between observation and theory in the bow shock system. This is the course the investigator has already set within the present study.

APPENDIX A

21333-6019-RU-00

PHENOMENOLOGY OF THE EARTH'S BOW SHOCK SYSTEM. A SUMMARY DESCRIPTION OF EXPERIMENTAL RESULTS

Eugene W. Greenstadt

Prepared for Summer Advanced Study School
"Magnetospheric Particles and Fields - 1975"

22 July 1975

Space Sciences Department
TRW Systems
One Space Park
Redondo Beach, California 90278

PHENOMENOLOGY OF THE EARTH'S BOW SHOCK SYSTEM. A SUMMARY DESCRIPTION OF EXPERIMENTAL RESULTS

ABSTRACT

The earth's bow shock may be viewed as part of a complex plasma system of field-particle interactions in which charged particle energy distributions are distorted from, and restored to, equilibrium, fields are severely perturbed, and waves are generated in a frequency range from 0 to more than 70 kHz. The system of perturbation causes and effects includes a central shock of radically-varying character, a vast upstream region of radiated, reflected, and created disturbance extending at least to lunar distance in the solar direction, and a downstream region of both order and turbulence flowing up to and around the magnetosphere. The observational data delineating the system as we know it are enumerated in terms of various field and particle components, most of which have been detected independently of each other, and an effort is made to coordinate some of the many disparate experimental results and describe, if not explain, them in relationship to one another.

INTRODUCTION

A customary way of studying the dynamics of a physical system is to arrange, theoretically or experimentally, a well-defined steady-state condition, introduce a perturbation, and observe or analyze the resulting modulations of the system. The earth's magnetosphere creates such a perturbation in the solar wind. Unfortunately, the interaction of the magnetosphere with the solar wind represents a case of "overkill" from the viewpoint of a physicist looking for a small perturbation to illuminate a simple dynamic change: the perturbation is an obstacle totally blocking part of the flow; the flow is not stationary and is faster than most wave velocities in the medium; the medium is anisotropic and supports more than one wavemode, and the wavemodes are dispersive. The result is a nonlinear, irreversible modulation of the solar wind centered around a bow shock wave of considerable complexity. Otherwise, the situation is ideal.

The complexity of the earth's bow shock system is actually close to ideal in one important sense. It offers the advantage of affecting an immense region of space with a rich assortment of collisionless plasma phenomena, almost all of which occur on scale large relative to spacecraft and their measuring devices. Thus a wide range of plasma behavior is accessible to satellite measurements. Indeed, the array of phenomena is so extensive that even the descriptive phase of bow shock investigation is still in progress as this is written, and detailed physical processes have only recently begun to reveal themselves quantitatively in well-defined contexts. This

report attempts to describe briefly the wealth of observed phenomena that constitute the bow shock system. It covers, and condenses in a few figures, the phenomena representing particle and field constitution and structure of the bow shock system, with the emphasis on items discovered by spacecraft observation. The MHD, or fluid-like, qualities of the earth's shock have already been treated fully (Spreiter et al., 1968) and the results extended to other planets throughout the solar system (Dryer et al., 1973; Dryer, 1975). This subject is not discussed here.

In the following sections, the description begins outside the nominal shock and proceeds inward through the shock to the magnetosheath. The latter receives relatively lean attention for reasons given in the appropriate paragraph. Macroscopic features of the system are presented first, then microscopic, the distinction being principally one of scale relative to the typical monotonic shock thickness c/ω_{pi}: microscopic phenomena take place within the gradients of macroscopic phenomena, involve waves of $\lambda \lesssim c/\omega_{pi}$, and exist on the fine scale where nonequilibrium features (e.g., nonmaxwellian components of particle distributions) are important and produce measurable effects.

MACROSTRUCTURE

FORESHOCK

Figure 1 summarizes the principal observed constituents, to date, of the upstream region in the ecliptic plane for a typical interplanetary field of angle $\theta_{XB} = 45°$. The approximate orbit of the moon is included as a circle at 60 R_E, since measurements by Explorers 33, 35 and by Apollo plasma probes placed on the lunar surface have played a significant role in acquiring the data contributing to the figure. The average asymmetric bow shock of Fairfield (1971) is used in the illustration.

Statistical studies have shown that for the 45° stream angle, various particle flows and field perturbations occur approximately in the sectors depicted. These will be enumerated individually. However, it will be necessary on occasion to refer to the entire conglomeration of upstream phenomena depicted in Figure 1 as a unit, so that a single term for this purpose would be useful. In this paper, the single word "foreshock" will be used to represent collectively any set or subset of effects associated with the presence of the shock but existing outside the magnetosheath proper. The foreshock is composed of numerous individual forerunners: protons, electrons, waves and their local interaction effects, that forewarn the solar wind of the approaching obstacle.

The fundamental relationship between the shock and foreshock revolves around the local field geometry at each point of the nominal shock "surface." Particles of high velocity parallel to $\underset{\sim}{B}_{SW}$ escape from the shock along $\underset{\sim}{B}_{SW}$

and occupy a region behind the field line tangent to the shock. Particles of less energy can escape only from points of the shock not near the tangent point of the field. The guiding centers of all the particles follow the field in the plasma frame and they interact with the fresh, oncoming solar wind to produce waves with various characteristics. In the earth's frame, the solar wind velocity must be added to the guiding center velocities vectorially, so the boundaries of different components of the foreshock (dashed lines S_e, S_p in Figure 1) are displaced from the field direction by appropriate angles. Because no particle escapes with infinite velocity, the overall foreshock boundary is necessarily behind the tangent field line, as illustrated.

The easiest escape is for thermal electrons, since the mean thermal velocity of electrons in the solar wind, at 1.5×10^5°K (Feldman et al., 1973; Scudder et al., 1973) is already about 2000 Km/sec. Heating of electrons takes place at their earliest contact with the shock gradient or at its foot (Montgomery et al., 1970; Neugebauer et al., 1971; Greenstadt et al., 1975), raising their energies from about 13 to 50 eV on average, but also creating electrons of 100 eV and more at the outermost limit of the shock structure (Neugebauer et al., 1971). These heated electrons, essentially still out in the solar wind, have velocities averaging about 4000 Km/sec and ranging well above 6000 Km/sec. They have no difficulty leaving the shock upwind along $\underset{\sim}{B}$ and, indeed, so many of them do that they reverse the usually antisolar electron heat flux (Feldman et al., 1973). Reverse-streaming electrons in the energy range 40-1000 eV are known to travel at least as far as the moon, where they are often observed during the lunar night (Reasoner, 1975). The electron forerunners support the growth of plasma oscillations near the electron plasma frequency $f \approx f_{pe}$ (Fredricks et al., 1971), and correlations of backstreaming electrons of $E > 700$ eV with electric waves have

been recorded (Scarf et al., 1971). In Figure 1, the morningside boundary S_e of the electron foreshock has been put at $\theta_{XS_e} = -49°$, following Feldman et al's minimal 4600 Km/sec velocity contributing to the reverse heat flux in one case. In reality, the boundary S_e is practically coincident with the tangent $\underset{\sim}{B}_{SW}$. The extent to which electrons of every given reverse velocity generate plasma oscillations has not been established, but it is recorded that electrons of $E < 100$ eV contribute most to the heat effect (Feldman et al., 1973) while only electrons of $E \gtrsim 700$-800 eV have been demonstrated to be associated with the presence of plasma oscillations, as already mentioned. Thus, there should perhaps be two separate lines for waves and heat flux, both closer to $\underset{\sim}{B}_{SW}$ than shown in Figure 1, but a single boundary S_e for both electrons and plasma waves has been drawn for simplicity, and to emphasize that the velocities are after all finite.

Within about 15° of the subsolar point (measured by θ_{XT}) a second forward boundary appears to be determined by protons traveling along $\underset{\sim}{B}_{SW}$ with guiding center velocity $U_{\|} > V_{SW}$ in the solar wind frame. It is customary to represent this velocity as a multiple $p\ V_{SW}$ of the solar wind velocity, and near the subsolar shock $p \approx 1.6$ (Diodato et al., 1975). The slope of the boundary S_p, determined by the vector sum $p\ V_{SW}\ (\underset{\sim}{B}_{SW}/B_{SW}) + \underset{\sim}{V}_{SW}$ is given in terms of p by the formula

$$\tan \theta_{XS} = p \sin \theta_{XB}/(p \cos \theta_{XB} - 1). \qquad (1)$$

The tangent with slope $\tan \theta_{XS}$ touches the nominal shock at about $\theta_{XT} \approx 7°$, where the local normal makes angle $\theta_{XB} \approx 50°$ with the typical $\underset{\sim}{B}_{SW}$ at $\theta_{XB} = 45°$. Thus, it is at $\theta_{Bn} \approx 50°$ that the shock appears to release protons for excape upstream. The corresponding angle θ_{XS_p} is 83° as depicted.

The protons streaming back from the shock are associated with magnetic waves of periods 10-100 seconds in the spacecraft frame, propagating in the solar wind and presumably doppler shifted from local proton cyclotron periods. It is these long period proton waves that have been most commonly observed and studied rather than the particles themselves. The existing documentation on these upstream waves has established such a consistent statistical picture of $73° \lesssim \theta_{XS_p} \gtrsim 83°$, regardless of solar wind conditions, that the concept behind equation (1), i.e., first order dependence of the forward wave boundary on a multiple p of the solar wind velocity ($U_{\parallel}$ proportional to V_{SW}), can hardly be doubted. Distant observations of the waves have given an average overall boundary compatible with the above angles (Fairfield, 1969; Diodato et al., 1975), while measurements close to the shock have demonstrated the local appearance of the waves when $\theta_{nB} \lesssim 45°$ both statistically (Formisano et al., 1973) and on a case-by-case basis (Greenstadt et al., 1970b; Greenstadt, 1972).

Polarization, frequency, and velocity characteristics of the upstream waves have been found to exclude the likelihood of their propagation from the shock, pointing to local generation by backstreaming particles as probable cause (Fairfield, 1969; Greenstadt et al., 1970b). Reverse flows of protons of approximately the right average $U_{\parallel}$ at the right angle have been reported statistically (Asbridge et al., 1968; Benson et al., 1975) and in individual cases (Asbridge et al., 1968), and individual correlations of waves with simultaneous backstreaming protons of about the right energy (4-7 keV) have been published (Scarf et al., 1970). A model has been proposed which predicts that reflection of solar wind protons from the bow shock, with attendant

acceleration by the interplanetary electric field, should give them energies compatible with those observed (Sonnerup, 1969), and models have also been proposed which predict upstream wave excitation by beams of reflected protons (Barnes, 1970; Fredricks, 1975). All the above results are summarized in Figure 1 by line S_p and the notations in the sector behind it. For the remainder of this paper, the long period upstream oscillations will be designated proton waves.

There are still more components of the foreshock than those already mentioned. Bursts of electrons of energy in excess of 30-40 keV, or electron "spikes," which commonly occur in or behind the shock (Fan et al., 1966; Anderson, 1969) also occur upstream with similar temporal behavior to those in the sheath (Fan et al., 1966; Anderson, 1968; Anderson, 1969). These bursts evidently travel along field lines as indicated by their statistical occurrence at lunar distance and have been attributed to a source just behind the bow shock, since their intensity is highest there (Anderson, 1969). Such suprathermal electrons have been seen in association with magnetic waves of about 10-second periods (Jokipii, 1968), but the evidence suggests that on balance they exist behind $\underset{\sim}{B}_{SW}$ and not S_p. This is the way they are indicated in Figure 1.

In addition to energetic electrons, there are energetic protons of energy 30-100 keV, and higher, streaming away from the shock (Lin et al., 1974; West and Buck, 1975). But here there is an interesting difficulty. Protons of such energies, corresponding to parallel velocities $\gtrsim 6\ V_{SW}$ should, like fast electrons, appear behind a line like S_e in Figure 1, not

much displaced, if at all, from the field line that guides them. Superficially they do not. Instead they seem to be confined to the same sector bounded by S_p, at least at lunar distances (Lin et al., 1974), and they have not been found to appear upstream in proper time sequence corresponding to their energies when the field line through the observation point suddenly makes fresh contact with the bow shock. These curious characteristics of reversed protons above 30 keV, together with some less compelling ones, led Lin et al. to the hypothesis that the energetic protons are created upstream from the shock rather than in the shock itself. Neither confirmation or disproof of the hypothesis has been advanced, but it seems worthwhile to consider another resolution of the problem.

The rejected idea of bow shock origin for high energy protons rests on the implicit assumption that the full range of reverse particle velocities should be produced and released simultaneously at the point of tangency either of $\underset{\sim}{B}_{SW}$ or S_p. The fastest ions would then certainly race back up the field line arriving at any upstream observation point both forward of and, for switch-on geometry, earlier than slower ones. This assumption carries the implication that whatever the shock does to, or for, protons of 3 keV at $\theta_{nB} \approx 50°$ it does also to, or for, protons of 100 keV. To state this another way, quasi-parallel, or marginally parallel shock geometry at $\theta_{nB} \approx 50°$ is not significantly different from fully parallel geometry at $\theta_{nB} \approx 0°$ as far as production or release of protons of differing energies is concerned. This does not seem likely in view of the radically changing magnetic structure of the shock as θ_{nB} goes from 50° to 0°.

A tentative resolution of the problem is proposed in Figure 2: Protons of energy 100 keV ($U_{\parallel} \approx 10\ V_{SW}$) leave the shock not where $\theta_{nB} = 50°$, but where $\theta_{nB} \approx 0°$, travel more or less along $\underset{\sim}{B}_{SW}$, as they should, and, in the steady state, arrive at lunar distance at about the same angle as protons of energy 3 keV. In the case of switch-on parallel geometry, it is suggested that if energetic protons are produced by multiple reflection as postulated in an earlier paper (Greenstadt, 1974), or by any repetitive process, it may take a few tens of seconds longer to generate 100 keV than 3 keV ions in the shock, which would explain the failure of the faster ones to arrive ahead of the slower ones. Exact coincidence in angle or time of arrival is of course not proposed seriously. However, approximate coincidence would easily be compatible with the uncertainties of measured or inferred angles, energies, and delays presently in the literature. Thus the Lin et al result can be taken as a possible clue to the pattern of particle energization in the quasi-parallel shock structure. This view appears to be supported by the strong correlation of 100 keV protons in the magnetosheath with enhanced field turbulence (West and Buck, 1975).

It must be noted that the 100 keV protons have been treated as part of the foreshock and discussed as if created in the shock, because of their pattern of occurrence. The site of their origin is by no means established, however, and they may be created deep in the sheath and merely released by the parallel configuration, or may indeed be generated upstream.

Two additional components of the foreshock remain, but these are perhaps more appropriately considered part of the micro, rather than macrostructure of the shock. They are plasma and electromagnetic waves in the frequency range of 1 Hz to 1 kHz. Electric noise at or around the proton

plasma frequency (.2-1.0 kHz) and electromagnetic noise between .1 and 1.0 kHz have been reported in connection with upstream proton waves and reflected 4-7 keV protons (Scarf et al., 1970; Neugebauer et al., 1971). The persistent occurrence of .5 - 4.0 Hz whistlers, generally but not exclusively, close to the shock has been established (Fairfield, 1974), and the existence of damped wave pockets, $f \approx .25$ Hz $\approx 2\text{-}4\ \Omega_p$ has been documented (Russell et al., 1971). All these wave constituents of the proton foreshock are associated with local field gradients, principally that of the shock itself, and also with the gradients of upstream proton waves.

Two important properties of the proton foreshock must finally be noted. First, it plays a significant role in the total shock system since proton forerunners have been reported to carry up to 40 percent of the energy density of the solar wind (Asbridge et al., 1968). It follows that the solar wind's parameters may at least on occasion differ appreciably inside and outside the foreshock. Second, the synoptic diagram of Figure 1 must be remembered as a symbolic black-and-white snapshot of a system that can be appreciated properly only if represented as a technicolor motion picture. The interplanetary field direction and the solar wind parameters are highly variable in time and the shock system is three-dimensional. Consequently the view obtained by a spacecraft or group of spacecraft at any instant, and the years of data from which the average picture of Figure 1 has been constructed, are often characterized by angles θ_{XB}, θ_{XS_e}, θ_{XS_p} and by foreshock constituents in relative proportions different from those of the figure. It has just recently been determined, for example, that if the interplanetary field is so oriented that the point of escape of reflected protons is on the flank of the bow shock rather than near the subsolar point, the boundary of the proton wave foreshock occurs at an angle compatible with

$p > 2$ instead of $p = 1.6$ (Diodato et al., 1975). Many other refinements of the foreshock picture undoubtedly remain to be discovered.

MIDSHOCK

The bow shock, for purposes of the most general discussion by an experimentalist, is best thought of as the physical entity between the magnetopause and the unaffected solar wind where large rates of change of field, density, and temperature occur. This pluralistic definition is unnecessary when there is one distinct gradient where upstream and downstream conditions are easily divided by all of the usual macroscopic diagnostics together; the definition is essential when diagnostic effects are separated and spread through a long observing interval.

The gross variability of shock profile implicit in the above equivocation results from variability, both temporal and spatial, of the local angle θ_{nB}. The sketch at the center of Figure 3 represents the basic dependence of shock magnetic structure on this angle. The density and field magnitude are represented vertically; $\underset{\sim}{B}$ is horizontal and could be directed in either sense. The nominal shock is represented for clarity as a quarter-circle concave with respect to the upstream field in the foreground. The real bow shock is of course convex and roughly hyperbolic.

Qualifications deferred, the shock transition is monotonic, where $\theta_{nB} \approx 90°$ (perpendicular shock). At $\theta_{nB} \lesssim 85°$, $M \lesssim 3$, and $\beta << 1$, a damped, standing whistler precursor develops ahead of the main gradient, which still forms a prominent and unmistakeable demarkation between upstream and downstream solar wind (Greenstadt et al., 1975a; Fairfield and Feldman, 1975). Under most conditions, the standing wave is negligible or absent, but a foot of slightly elevated B appears at the base of the shock ramp. At $\theta_{nB} \approx 50°$,

equivalent at the subsolar point to $p \approx 1.6$, the shock begins to "relax:" almost periodic oscillations, or "pulsations," develop whose amplitudes are comparable to the monotonic gradient for $\theta_{nB} \gtrsim 50°$, and the shock becomes irregular and difficult to distinguish as a single transition (Greenstadt et al., 1970a,c; Fairfield, 1974). In the range $0° \lesssim \theta_{nB} \lesssim 50°$, the shock appears to consist of a train of semi-periodic oscillations of tens of seconds period and both large and small amplitudes, often alternating in groups of a few cycles each, mixed with irregular fluctuations of large amplitudes and shorter periods (Greenstadt et al., 1970a). The entire train appears to have a length, or "thickness," exceeding 2 R_E along the local normal (Greenstadt, et al., 1970a; 1975b) and is probably much thicker. By large amplitude it is meant that the oscillations may have peaks and troughs at field values higher than, even double, the expected magnetosheath field level, and lower than the solar wind field level, even as low as zero. The two basic shock structural signatures corresponding to the two angle ranges $\theta_{nB} = 90°$-$50°$, $50°$-$0°$ have been designated quasi-perpendicular and quasi-parallel.

The appearances of both quasi-parallel structure and proton foreshock at angles 45°-50° are not the results of statistical coincidence. Observation indicates a 1-1 correspondence (Greenstadt et al., 1970a), while a "pulsation index" designed to test for q-parallel structure using the orientation of $\underset{\sim}{B}_{SW}$ has been repeatedly successful within existing experimental uncertainties when the value $p = 1.6$ associated with the approximate proton wave boundary has been used in the calculation (Greenstadt, 1972).

The proton foreshock is thus an extension, or an integral part, of the quasi-parallel shock, and, in a loose sense, the converse also must hold, i.e., the foreshock so modifies the incoming solar wind that at least some of the characteristics of the "shock" are derived from the foreshock's existence upstream. One example often cited is the possible amplification of upstream waves at the shock (McKenzie and Westphal, 1968), an effect that might contribute to creation of the very large amplitude q-parallel pulsations.

The integral connection between upstream proton waves and q-parallel macrostructure is manifested partly as an experimental ambiguity in which it can become impossible to decide where upstream ends and downstream begins. Observations of individual cases convey the impression that the appearance of the q-parallel signature is accompanied by shock expansion (Greenstadt et al, 1970c; 1975b), but statistical analysis indicates that the average shock location moves inwards by about 1 R_E when q-parallel conditions prevail (Auer, 1974). Since the individual case studies referred to the "envelope" of the shock, meaning the most distant bursts of pulsations of amplitude comparable to the nominal shock jump, while the statistical study referred to jumps in ten-minute averages of field, these complementary results suggest that q-parallel geometry erodes the shock, allowing some of the otherwise static field energy to be distributed upstream as waves. A compatible statistical result by Formisano et al. (1973) using plasma data to define the shock showed that the spread in bow shock positions with respect to the average location increased when upstream waves were present. These studies demonstrate the ambiguity and diagnostic dependence of shock identification when $\theta_{nB} \lesssim 50°$.

The three-dimensional sketches around the lower part of Figure 3 represent typical proton velocity distributions at various points with respect to the shock. To interpret these, imagine the solar wind plasma flux emanating, without loss of density, from the near apex of the central figure so the flow is normal to the nominal shock everywhere. At left the flow is across the field, at right, parallel to it. The sketches are conceptual only; no attempt has been made to scale the thermal spread in velocity precisely to the solar wind velocity. Neither has each surface been constructed carefully to enclose a volume equaling the correct relative density.

At lower left, the average cool solar wind protons have density $\approx$ 4-5 cm^{-3}, thermal velocity about 40 Km/sec (7×10^{4}°K; Diodato et al., 1974; Formisano et al., 1974), and anisotropy $T_{\parallel}/T_{\perp} \approx 2$ (Feldman et al., 1974). Behind the quasi-perpendicular shock, at upper left, the velocity has been reduced 20 percent, the density has more than doubled, and the thermal velocity trebled (Formisano et al., 1973a), and the distribution has become flat-topped, with a variable, secondary peak and a high velocity nonmaxwellian tail (Montgomery et al., 1970). The secondary maximum has been drawn at about 2 V_{SW} in all directions, and the central peak more or less isotropically, but the degree of symmetry has not actually been established for either. Further downstream the distribution, not shown, becomes smoother and rounder at the peak, but the nonmaxwellian tail remains, and seems to extend (anisotropically) to protons up to 100-200 keV (10-14 V_{SW}) and beyond (West and Buck, 1975), implying that particles of very high energy are produced in or around the shock and carried downstream with the solar wind.

In the central figure, the vertical scale at right was marked parenthetically with density (N) as well as B because the ratios of downstream to upstream densities are similar to the field ratios (Formisano et al., 1973a). The vertical dimension can also represent temperature (T), but post-shock proton temperatures are typically an order of magnitude, rather than a factor of two or three higher than in the solar wind (Formisano et al., 1973a), as shown on the scale at left. Density and temperature are parenthesized because in q-parallel structures particle energy spectra form neither maxwellian, smooth, nor precisely repeatable distributions of any kind (Greenstadt et al., 1970a), so that the available data on temperature and density have been obtained from computer-constructed approximations. Also, the spectral sweep period of existing instrumentation is slower than many large amplitude oscillations and it is by no means established that density and temperature fluctuations follow field oscillations in detail, although they are elevated on average where the pulsations are present (Greenstadt et al., 1975b).

In the sketch at lower right, solar wind protons penetrating the proton foreshock are slowed slightly, about 30 Km/sec (Formisano and Amato, 1975), have their anisotropy reduced 10 percent or so (Feldman et al., 1974), and encounter another group of protons traveling upwind along $\underset{\sim}{B}_{SW}$ at about double the solar wind speed (preceding Section). This group evidently includes a nonmaxwellian high energy wing of protons up to 100 keV or more (West and Buck, 1975). The flow and/or its anisotropy fluctuate in direction synchronously with the long period proton waves (Greenstadt et al., 1968; Scarf et al., 1970).

The rather fanciful distribution illustrated at the right is intended to convey the following composite characteristics of the solar wind in the midst of the quasi-parallel magnetic pulsation structure: 1. The bulk speed is substantially unaffected; 2. the peak of the distribution is reduced in density; 3. the "temperature" is raised, i.e., protons from the peak of the distribution are scattered in direction and acquire high velocities; 4. overall (averaged) distributions are multimodal and irregular in time, and the exact form of distribution at any given position and instant is wholly unknown (hence the question mark); 5. the flow is severely deviated in direction by large amplitude transverse waves; 6. the flux accompanying small magnetic upstream-like waves in between bursts or trains of pulsations is deviated from the normal solar wind direction, possibly from having passed through "detached" bursts of pulsations further upstream. The foregoing list of features of q-parallel plasma structure is taken from a recently completed study of a nearly geometrically parallel shock ($\theta_{nB} \approx 10°$; Greenstadt et al., 1975b) and may give an exaggerated picture of conditions in a structure where $20° \lesssim \theta_{nB} \lesssim 50°$.

Downstream from the q-parallel shock the details of macroscopic structure have not been defined experimentally by case study or multiple spacecraft observations, and no sketch is offered. It has been determined statistically from single-spacecraft observations that the proton distributions have velocity reduced by about the same amount on average as behind the q-perpendicular shock and that the temperature and density jumps are lower, $T_{p2}/T_{p1} \approx 3.2$, $N_{p2}/N_{p1} \approx 2$; also the distributions appear to be more nearly maxwellian, lacking a high energy tail (Formisano et al., 1973).

The known effects of the shock-encounter on the electron component of the solar wind plasma are conceptualized in Figure 4 according to the same pattern as in Figure 3. At lower left, the electrons are slightly anisotropic and hotter than the protons, to begin with; note the overall difference in scale. At far left, inside and just behind the q-perpendicular shock, the electrons are heated to a "temperature" four times the upwind value, but the distribution is nonmaxwellian, with a broad flat top. At right, in the electron foreshock, electrons are heated and the net heat flux is back upstream. Detailed data on electron behavior in or behind the q-parallel pulsations are not available and no sketch is included. It is reasonable to surmise that the electrons are heated at the outermost large gradient. The suprathermal electron spikes reported by Anderson (1969) were concentrated most heavily in or behind the nominal shock ramp, but it is not known whether they constitute a wing of the post shock electron distribution or a separate phenomenon related to q-perpendicular or q-parallel structure.

The description of the bow shock just given is based on numerous studies, many statistical, but most of which made no differentiation among shock crossings for differing upstream plasma conditions. Thus, some enumerated features may exist only at some times or may be mixtures of features that don't really occur together in any single case. In the average solar wind at 1 AU, the magnetosonic mach number $M_{MS} = V_{SW}/(C_A^2+C_S^2)^{1/2} \approx 4.5\text{-}8.0$, and $\beta = 8\pi Nk(T_p+T_e)/B^2 \approx 1$ (Formisano et al., 1974), where C_A and C_S are Alfvén and sonic speeds. These are the values assumed to be applicable when most of the data contributing to the "typical" shock profiles presented above were acquired. However, β and M_{MS} and, even more, M_A, are occasionally much lower

or higher than their average values, so that the shock description must be appropriately qualified.

If $1 < M_A \lesssim 3$ and $\beta \lesssim .1$, the shock is "laminar," appearing as an extremely simple magnetic profile. Usually there are some nearly periodic waves standing upstream or visible in the ramp and just behind it when $50° \lesssim \theta_{nB} \lesssim 88°$ (Greenstadt et al., 1975a; Fairfield and Feldman, 1975). The downstream proton distributions tend to be maxwellian and do not exhibit secondary peaks or high velocity tails (Formisano et al., 1973a). The secondary peaks are evidently associated with shocks where $M_A \gtrsim 3$ (Formisano and Hedgecock, 1973). The monotonic ramp of the q-perpendicular shock gives way to a highly irregular train of waves and pulses when $\beta >> 1$; field increases in the sharply peaked waves reach extraordinary levels 20 times the upstream field value, so that the high-β condition may be eliminated locally within the structure and even the formation of a steady state shock may be questionable (Formisano et al., 1975).

The gross effects of M and β on shock structure are summarized in a classification scheme devised by Dobrowolny and Formisano (1973). (Some examples were illustrated by Greenstadt, 1974a.) The classification is as follows, for quasi-perpendicular shocks:

Parameter Values	Type of Shock	Name of Structure	Macroscopic Features of Bow Shock
$\beta << 1$, $M \lesssim 3$	Cold plasma, low Mach no.	LAMINAR	Clean field jump, sometimes with damped periodic waves, no turbulence; Relatively little proton temperature jump ($T_{p2}/T_{p1} \approx 2$) maxwellian downstream distribution.

Parameter Values	Type of Shock	Name of Structure	Macroscopic Features of Bow Shock
$\beta \approx 1$, $M \gtrsim 3$	Cold plasma, high Mach no.	QUASI-LAMINAR	Clean field jump, downstream nearly-periodic waves, little turbulence; appreciable proton temperature jump, bimodal distribution, nonmaxwellian high energy tail downstream.
$\beta \approx 1$, $M \lesssim 3$	Warm plasma, low Mach no.	QUASI-TURBULENT	Clean field jump, small-scale turbulence; Little proton temperature rise, maxwellian downstream distribution.
$\beta \approx 1$, $M \gtrsim 3$	Warm plasma, high Mach no.	TURBULENT	Irregular field fluctuations obscuring definite average field jump; Bimodal or multimodal proton distributions, nonmaxwellian downstream.

In the table, the dividing value $M \approx 3$ is the experimentally-determined value approximating the critical Mach number known in laboratory shock studies (Paul, 1969). It is not known to what extent the distinctions in the table apply under q-parallel geometry, but strictly local combinations of parameters may play an important role in defining the processes taking place in local gradients.

AFTERSHOCK

Downstream from the earth's bow shock a modified, heated solar wind flows around the magnetosphere, forming the magnetosheath. The structural properties of the magnetosheath have not been well defined experimentally for two reasons: first, plasma detectors have not generally had the time- and

angle-resolution needed there, and second, the magnetosheath cannot be explored reliability with a single satellite. The time lapse between measurements made by the same spacecraft deep in the magnetosheath and in or outside the shock is rarely less than three or four hours, usually much more, which is longer than the typical interval between changes in solar wind parameters. Thus separation of spatial from temporal variations is effectively ruled out. Discussion of the far downstream structure is therefore confined here to a few remarks regarding direct involvement of the shock.

The magnetosheath has been described as both "tangled" and "more ordered than the interplanetary field" with emphasis on the latter (Fairfield, 1967), but the impression seems to persist widely that the sheath is "turbulent." This impression needs to be corrected. Field fluctuations of amplitude 10-20 percent of the average field are often present in the sheath, imposed on a well defined average magnitude and direction, and are commonly made up of many nearly periodic wavetrains. Moreover, the plasma spectra accompanying such fluctuations are, on average, quite reproducible from one to the next (Greenstadt et al., 1968; 1975b). Thus the sheath is not inherently turbulent, although it may be said that moderate turbulent fields exist in it. The power levels of field fluctuations with $f < .2$ Hz do vary by an order of magnitude or more from one satellite pass to the next (Fairfield and Ness, 1970), but when the field noise level is truly high in the sheath, relative to the field, the record looks very much like it does in the q-parallel shock and in fact is reliably accompanied by suprathermal protons which appear and disappear almost always synchronously with the appearance and disappearance of the large amplitude "turbulence" (West and Buck, 1975).

It is suggested here that the sheath, even far behind the shock, merely responds, with an appropriate delay, to the upstream parameters governing shock structure. The magnetosheath then, except for extreme conditions of very high solar wind, may really never be turbulent behind a clearly definable shock transition. When it appears so, the inner portion of the q-parallel pulsation structure may have simply expanded downstream to include the point of observation and the question of the structure of the sheath may have become moot, the sheath and shock having become indistinguishable within a broad irregular transition, or relaxation shock (Auer and Völk, 1973).

Statistically, the magnetosheath behaves like a region whose nonstatic magnetic oscillations are derived from, and dependent on, local shock conditions. Higher transverse mode power levels are found more often on the dawn (where $\theta_{nB} < 50°$) than the dusk side, more often near the shock than deep in the sheath (but also near the magnetopause), and more often behind the subsolar shock (where M is highest) than along the flanks (Fairfield and Ness, 1970). Power levels decline exponentially with distance from the sun-earth line (Mariani et al., 1970) in the sheath, and the transverse wave polarizations tend to be aligned parallel to the shock (Fairfield and Ness, 1970). The most important characterizations of the sheath have not been determined, however. These are: 1. the pattern and level of magnetic and electric fluctuations, and 2. the particle energy distributions throughout the region, when any given solar wind condition prevails.

MICROSTRUCTURE

QUASI-PERPENDICULAR GEOMETRY

The transition from upstream to downstream plasma states when $90° < \theta_{nB} \lesssim 50°$ occurs in the plasma frame in a distance between c/ω_{pe} (Fredricks et al., 1970) and about 10 c/ω_{pi} (Ossakow et al., 1970; Greenstadt et al., 1975a; Fairfield and Feldman, 1975), the thicker transitions accompanying the smaller angles. Because of the wide variation of N_{SW} from roughly .5 to > 20 cm^{-3} (Formisano et al., 1974), shock thicknesses can vary from 1 to 3000 km, and may appear even greater to a spacecraft because of shock motion. The wider thicknesses are taken here to include a few cycles of standing waves, when present upstream from a final "ramp," in low Mach number, oblique cases where the wavelength of each cycle, and the ramp itself, may be 1-2 c/ω_{pi} or so. The thickness is also taken to include any foot which may be appended to the ramp upstream.

The standing waves and foot are included as part of the shock because some of the heating effects of the shock on the solar wind occur there. The gradients of standing waves are associated with drift velocities which, while less than the drift in the main gradient, should be sufficient to trigger ion acoustic waves at low β and scatter electrons. Where standing waves are absent or negligible, electrons are scattered and energized at the foot of the ramp and in upstream (q-parallel) proton waves where field gradients are only small to moderate (Montgomery et al., 1970; Neugebauer et al., 1971; Greenstadt et al., 1975a). In fact, the bulk of electron scattering is accomplished by the time half the ramp has been traversed by the plasma,

although the process is incomplete until the wind is further downstream behind the shock (same references above).

The protons (and α's) are retarded slightly and contain a group of ions at $\approx 2\ V_{SW}$ before midramp, as the initial electron scattering takes place (Neugebauer, 1970; Montgomery et al., 1970). The bulk of electrons are accelerated at the same time, evidently because of a charge-separation electrostatic potential parallel to the flow, i.e., normal to the shock (Neugebauer, 1970). The electrons are largely thermalized by midramp, and the protons are then strongly and quickly thermalized just at or after midramp in a distance of 1-5 c/ω_{pi} (Ossakow et al., 1970). Both electrons and protons display flat-topped distributions when heated. The flat, or even concave, electron distribution persists downstream in the magnetosheath (Montgomery et al., 1970; Scudder et al., 1973).

The sequence of events just described is exhibited qualitatively in Figure 5. No attempt has been made to scale the distribution function of protons and electrons to each other, and they are shown conceptually only. The magnetic shock profile illustrated may be taken as representing a "typical" q-perpendicular case with $\beta \approx 1$, $M > 3$. The typical behavior of T_e/T_p is shown just above the distribution sketches: the ratio, a little over 2 in the solar wind, rises quickly to about 8-10 when the electrons are heated, and drops quickly to less than 1 when the protons are thermalized.

The remaining two panels at the top of Figure 5 represent the electric and magnetic wave noise that accompanies the particle events in the ramp.

Electrostatic waves at or around the electron plasma frequency in the 15-30 kHz range appear ahead of the ramp, generally where there are 100-800 eV electrons (Scarf et al., 1971; Neugebauer et al., 1971). Electrostatic oscillations of a few hundred to a few thousand Hz appear above background (≈ 10 μV/m) at the foot of the ramp, reach a peak intensity of 1-10 mV/m at midramp and subside to a lower level downstream (Fredricks et al., 1970; Rodriquez and Gurnett, 1975). Detailed study of the lower frequency band of electric oscillations has shown that it may consist of numerous bursts of nearly monochromatic waves at many individual frequencies (Fredricks et al., 1970).

Electromagnetic noise in the whistler mode, highest in intensity at midramp, is found below the local electron cyclotron frequency which rises with B through the shock (Smith et al., 1967; Greenstadt et al., 1975a). There is also a distinct band of magnetic waves, generally with f ≈ 1 Hz and .3 Hz ahead of and behind the main ramp gradient, respectively, in about 85 percent of observations (Olson and Holzer, 1974).

The typical, or average, case just described differs in detail from many individual examples of the bow shock. Some sorting of the variability of microstructural details has been effected by examination of cases with differing β's and M's (Formisano, 1974; Greenstadt, 1974a). Figure 6 sketches the general outline of variation of electric and magnetic noise as functions of these parameters. There seems to be an increase in the electromagnetic noise power P_B with rising β, shown on the left side of the diagram. Quantitatively, the results so far are tenuous, but measurements in a few cases have indicated power levels some 6 times higher when β > 10 (Formisano et al.,

1975) than when $\beta \approx .1$ (Greenstadt et al., 1975a). The scale at left applies only to $f \approx 10$ Hz; since the electromagnetic spectrum tends to fall as f^{-3} or f^{-4} (Smith et al., 1967; Olson et al., 1969; Rodriguez and Gurnett, 1975), the power spectral density at other frequencies must be proportioned accordingly. The integrated average power in the shock between 1 and 140 Hz was found to be about 4×10^{-11} ergs/cm^3 (Olson et al., 1969); presumably $\beta \approx 1$ for most of the cases contributing to that estimate.

Electrostatic noise is represented on the right side of the diagram of Figure 6 in terms of the peak rms field strength below $f \approx 3$ kHz, where the principal plasma wave component occurs (Fredricks et al., 1970; Rodriguez and Gurnett, 1975). Peaks are typically on the order of 1 mV/m and 10 mV/m for low and high Mach number shocks (Formisano, 1974; Greenstadt, 1974a) and readings of tens of mV/m have been recorded during exceptional high M crossings. Estimates of integrated electrostatic wave energy require cautious interpretation because of the presence of many discrete frequencies (Fredricks et al., 1968) but instantaneous ratios of electric to magnetic energy density E_E/E_B have been found to range up to 5×10^2 (Rodriguez and Gurnett, 1975).

The overall message of Figure 6 is that microscale magnetic and electric wave activity are somewhat independent of each other, but are both low for the bow shock in cold, low M solar wind flow and both high for the bow shock in hot, high M solar wind flow. The variation of P_B with β has not revealed any inflections, but the Mach number dependence of <E> appears to undergo a significant change at $M \approx 3$. This is a reasonable phenomenon to expect since it is plasma waves that presumably supply the electric fields needed to

scatter and heat both electrons and protons in the shock transition, in the absence of particle collisions, and the critical Mach number at which resistive dissipation by drift current instabilities becomes inadequate is at $M \approx 3$. Thus when $M \gtrsim 3$ either a different, more potent wave mechanism or two separate mechanisms operate to produce higher dissipation than is required when $M \lesssim 3$.

The identification of specific wavemodes responsible for the observed electric waves has not proceeded very far to date. There are several candidate instabilities that would yield observed frequencies under the conditions that prevail in the bow shock (Fredricks et al., 1970; Greenstadt and Fredricks, 1974). Certainly the ion acoustic mode is a likely noise source, and some recent work with laminar shocks seems to favor this mode heavily at the source of electron heating in simple cases (Morse and Greenstadt, 1975). When the measured thicknesses of several laminar crossings are used to estimate the electron drift velocities in the ramps, the results fall on or near the ion-acoustic stability/instability boundaries. Figure 7 shows the parametric locations of four selected cases with respect to the stability boundaries A and B of Manheimer and Boris (1972) and Fried and Gould (1961), the latter as represented in Tidman and Krall (1971); in the figure, $V_d/C_e = \frac{\Delta B}{\mu_o Ne\Delta S} \sqrt{\frac{2kT}{m_e}}$. The uncertainty flags represent estimated imprecision in the measurements of density. Within the ranges of uncertainties of the remaining plasma parameters, all four cases fell essentially along the Fried and Gould curve. Reliable differentiation between the two versions of the boundary is not possible from these few examples, but the

validity of the concept behind either model is clearly supportable for the coordinate values of these cases. Moreover, the results can be translated into an effective collision frequency $\nu_{eff} \approx \omega_{pi}$.

The laminar examples used in the above result all had $\beta \lesssim .1$. However, the cross-field ion acoustic mode becomes improbable when $\beta \approx 1$ (Wu and Fredricks, 1972), so this result cannot be generalized to the case of the average bow shock. Nevertheless, the many observations of early electron heating followed by proton scattering later in the structure suggest two separate mechanisms operating in the typical warm plasma, supercritical, quasi-perpendicular structure.

QUASI-PARALLEL GEOMETRY

Relatively little microscale information has been developed for the q-parallel structure, and only one case has been analyzed in detail (Greenstadt et al., 1975b), so generalization is impossible. The case examined was nearly parallel ($\theta_{nB} \simeq 10°$) and under almost typical conditions upstream, with β,M = .6, 3.9, a little below average. In contrast to the monotonic q-perpendicular shock, there were numerous large field gradients (large amplitude pulsations), many of which exceeded that of a typical q-perpendicular ramp, yet plasma wave noise generally remained below 1 mV/m, with only a few spikes reaching as high as several mV/m. The magnetic noise peaked repeatedly at or just above $10^{-2}\gamma^2$/Hz at 10 Hz. The multimodal proton distributions (Figure 3) were moderately reproducible in general outline, and an average of all distributions in the pulsation structure produced a spectrum clearly characteristic of neither the solar wind nor the magnetosheath

(Greenstadt, 1974a). The most interesting observation was of an "interpulsation" regime in which the magnetic field between bursts of pulsations gave the appearance of the proton wave foreshock, including the same average field magnitude as in the solar wind, but in which protons were scattered and magnetic and electric wave noise levels were elevated above solar wind background, often as high as in the laminar shock ramp. The enhanced wave noise levels appeared at frequencies typical of whistler and ion-acoustic modes associated with laminar shocks. The data did not support the proposition that the firehose instability (Auer and Völk, 1973) played a major role in maintenance of the structure in the case studied.

APPRAISAL

The survey of observational bow shock phenomenology given above conveys the wide range of ways in which the magnetosphere's disturbance of the solar wind is manifested. The microscopic aspects of the perturbations are of course the ones that make the system worth investigating, for the processes by which the medium departs from or returns to equilibrium are the basic subjects of collisionless plasma physics. The macroscopic phenomena enumerated are essentially diagnostic elements for discerning the microscopic processes that create them.

When viewed as a system the bow shock, if properly exploited, is seen to offer the classical means of examining perturbation effects despite the overall nonlinear, supersonic character of the solar wind interaction. The foreshock and laminar shock offer simple and almost linear cases of wave-particle interaction: electron-drift instability, beam (two-stream) instability, and firehose instability, some on the level of the ideal small perturbation. The quasi-perpendicular shock offers, at critical Mach number, a view of the mechanism by which effective viscosity begins to take over from effective resistivity and dispersion in limiting growth of the ramp, and, at supercritical Mach numbers, a view of the full nonlinear processes of overturning, trapping, and wavemode coupling. The quasi-parallel shock offers a view of the effects of dispersion superposed on all the other effects and of the local results of solar wind modification by the foreshock.

Three keys must be applied together to unlock the treasury of answers to microscale plasma processes provided by the bow shock system. These are:

1. A complete description of the unperturbed solar wind approaching the system;

2. High resolution, omnidirectional observation of proton and electron energy spectra from 10 eV to 100 keV and 10 eV to 1 MeV, respectively;

3. High resolution measurements of electric and magnetic waves from dc to 100 kHz.

We may hope that these keys will be created and employed properly in the future. Meanwhile, much information can still be obtained from the macroscopic behavior of field and particle diagnostics. Of particular interest would be the spatial patterns of full proton energy distributions in the foreshock and the magnetosheath, the coordination of upstream parameters with local magnetosheath structure, and the collection of shock profiles corresponding to as many different upstream parameter combinations as existing instrumentation can furnish.

ACKNOWLEDGMENT

This document was prepared under National Aeronautics and Space Administration Contract NASW-2398. Conversations with Drs. F. L. Scarf and C. T. Russell were valuable.

REFERENCES

Anderson, K. A.: 1968, J. Geophys. Res., 73, 2387.

Anderson, K. A.: 1969, J. Geophys. Res., 74, 95.

Asbridge, J. R., Bame, S. J., and Strong, I. B.: 1968, J. Geophys. Res., 73, 5777.

Auer, R. D.: 1974, J. Geophys. Res., 79, 5121.

Auer, R. D., and Völk, H. J.: 1973, Astrophys. & Space Sci., 22, 243.

Barnes, A.: 1970, Cosmic Electrodyn., 1, 90.

Benson, J., Freeman, J. W., Hills, H. K., and Vondrak, R. R.: 1975, The Moon, in press.

Diodato, L., Moreno, G., Signorini, C., and Ogilvie, K. W.: 1974, J. Geophys. Res., 79, 5095.

Diodato, L., Greenstadt, E. W., Moreno, G., and Formisano, V.: 1975, submitted to J. Geophys. Res.

Dobrowolny, M., and Formisano, F.: 1973, Rev. Nuovo Cim., 3, 419.

Dryer, M.: 1975, Exploration of the Outer Solar System, MIT Press, Cambridge, Ed. E. W. Greenstadt, in press.

Dryer, M., Rizzi, A. W., and Shen, Wen-Wu: 1973, Astrophys. & Space Sci., 22, 329.

Fan, C. Y., Gloeckler, G., and Simpson, J. A.: 1966:, J. Geophys. Res., 71, 1837.

Fairfield, D. H.: 1967, J. Geophys. Res., 72, 5865.

Fairfield, D. H.: 1969, J. Geophys. Res., 74, 3541.

Fairfield, D. H.: 1971, J. Geophys. Res., 76, 6700.

Fairfield, D. H.: 1974, J. Geophys. Res., 79, 1368.

Fairfield, D. H., and Ness, N. F.: 1970, J. Geophys. Res., 75, 6050.

Fairfield, D. H., and Feldman, W. C.: 1975, J. Geophys. Res., 80, 515.

Feldman, W. C., Asbridge, J. R., Bame, S. J., and Montgomery, M. D.: 1973, J. Geophys. Res., 78, 3697.

Feldman, W. C., Asbridge, J. R., and Bame, S. J.: 1974, J. Geophys. Res., 79, 2773.

Formisano, V.: 1974, Correlated Interplanetary & Magnetospheric Observations, D. Reidel-Dordrecht, Holland, Ed. D. E. Page.

Formisano, V., and Hedgecock, P. C.: 1973a, J. Geophys. Res., 78, 3745.

Formisano, V., and Hedgecock, P.C.: 1973b, J. Geophys. Res., 78, 6522.

Formisano, V., Moreno, G., Palmiotto, F., and Hedgecock, P. C.: 1973a, J. Geophys. Res., 78, 3714.

Formisano, V., Hedgecock, P. C., Moreno, G., Palmiotto, F., and Chao, J.: 1973b, J. Geophys. Res., 3731.

Formisano, V., Moreno, G., and Amato, E.: 1974, J. Geophys. Res., 79, 5109.

Formisano, V., and Amato, E.: 1975, submitted to J. Geophys. Res.

Formisano, V., Russell, C. T., Means, J. D., Greenstadt, E. W., Scarf, F. L., and Neugebauer, M.: 1975, J. Geophys. Res., in press.

Fredricks, R. W.: 1975, J. Geophys. Res., 80, 7.

Fredricks, R. W., Kennel, C. F., Scarf, F. L., Crook, G. M., and Green, I. M.: 1968, Phys. Rev. Lett's., 31, 1761.

Fredricks, R. W., Crook, G. M., Kennel, C. F., Green, I. M., Scarf, F. L., Coleman, Jr., P. J., and Russell, C. T.: 1970, J. Geophys. Res., 75, 3751.

Fredricks, R. W., Scarf, F. L., and Green, I. M.: 1972, J. Geophys. Res., 77, 1300.

Fried, B. D., and Gould, R. W.: 1961, Phys. Fluids, 4, 139.

Greenstadt, E. W., Green, I. M., Inouye, G. T., Hundhausen, A. J., Bame, S. J., and Strong, I. B.: 1968, J. Geophys. Res., 73, 51.

Greenstadt, E. W., Green, I. M., Inouye, G. T., Colburn, D. S., Binsack, J. H., and Lyon, E. F.: 1970a, Cosmic Electrodyn., 1, 160.

Greenstadt, E. W., Green, I. M., Inouye, G. T., Colburn, D. S., Binsack, J. H., and Lyon, E. F.: 1970b, Cosmic Electrodyn., 1, 279.

Greenstadt, E. W., Green, I. M., Inouye, G. T., Colburn, D. S., Binsack, J. H., and Lyon, E. F.: 1970c, Cosmic Electrodyn., 1, 316.

Greenstadt, E. W.: 1972a, J. Geophys. Res., 77, 1729.

Greenstadt, E. W.: 1972b, J. Geophys. Res., 77, 5467.

Greenstadt, E. W.: 1974, Solar Wind Three, Inst. Geophys. & Planet. Phys., University of California, Los Angeles, 440.

Greenstadt, E. W.: 1975, The Magnetospheres of Earth and Jupiter, D. Reidel-Dordrecht, Holland, Ed. V. Formisano, in press.

Greenstadt, E.W., and Fredricks, R. W.: 1974, Magnetospheric Physics, D. Reidel-Dordrecht, Holland, Ed. B. M. McCormac, 355.

Greenstadt, E. W., Russell, C. T., Scarf, F. L., Formsano, V., and Neugebauer, M.: 1975a, J. Geophys. Res., 80, 502.

Greenstadt, E. W., Russell, C. T., Formisano, V., Hedgecock, P. C., Scarf, F. L., Neugebauer, M., and Holzer, R. E.: 1975b, J. Geophys. Res., 80, in press.

Jokipii, Jr.: 1968, J. Geophys. Res., 73, 931.

Lin, R. P.: 1974, J. Geophys. Res., 79, 489.

Mariani, F., Bavassano, B., and Ness, N. F.: 1970, J. Geophys. Res., 75, 6037.

McKenzie, J. F., and Westphal, K. O.: 1968, Phys. Fluids, 11, 2350.

Montgomery, M. D., Asbridge, J. R., and Bame, S. J.: 1970, J. Geophys. Res., 75, 1217.

Morse, D. L., and Greenstadt, E. W.: 1975, Trans. Amer. Geophys. Union (EOS) Abstract 56, 433.

Neugebauer, M.: 1970, J. Geophys. Res., 75, 717.

Neugebauer, M., Russell, C. T., and Olson, J. V.: 1971, J. Geophys. Res., 76, 4366.

Olson, J. V., Holzer, R. E., and Smith, E. J.: 1969, J. Geophys. Res., 74, 4601.

Olson, J. V., and Holzer, R. E.: 1974, J. Geophys. Res., 79, 939.

Ossakow, S. L., Sharp, G. W., and Harris, K. K.: 1970, J. Geophys. Res., 75, 6024.

Paul, J. W. M.: 1969, Spec. Publ. 51, ESRO, Frascati, Italy, 97.

Reasoner, D. L.: 1975, J. Geophys. Res., 80, 187.

Rodriguez, P., and Gurnett, D. A.: 1975, J. Geophys. Res., 80, 19.

Russell, C. T., Childers, D. D., and Coleman, Jr., P. J.: 1971, J. Geophys. Res., 76, 845.

Scarf, F. L., Fredricks, R. W., Frank, L. A., Russell, C. T., Coleman, Jr., P. J., and Neugebauer, M.: 1970, J. Geophys. Res., 75, 7316.

Scarf, F. L., Fredricks, R. W., Frank, L. A., and Neugebauer, M.: 1971, J. Geophys. Res., 76, 5162.

Scudder, J. D., Link, D. L., and Ogilvie, K. W.: 1973, J. Geophys. Res., 78, 6535.

Smith, E. J., Holzer, R. H., McLeod, M. G., and Russell, C. T.: 1967, J. Geophys. Res., 72, 4803.

Sonnerup, B. U. Ö.: 1969: J. Geophys. Res., 74, 1301.

Spreiter, J. R., Alksne, A. Y., and Summers, A. L.: 1968, Physics of the Magnetosphere, D. Reidel-Dordrecht, Holland, Ed. R. L. Carovillano, 301.

Tidman, D. A., and Krall, N. A.: 1971, Shock Waves in Collisionless Plasmas, John Wiley-Interscience, New York.

West, H. I., and Buck, R. M.: 1975, J. Geophys. Res., 80, in press.

Wu, C. S., and Fredricks, R. W.: 1972, J. Geophys. Res., 77, 5585.

FIGURE CAPTIONS

Figure 1. Observed components of the foreshock in an ecliptic plane cross section with the interplanetary field at 45° stream angle. Subscripts e, p refer to electrons and protons. Components shown inside the lunar orbit were discovered by earth satellites, generally at distances up to about 35 R_E; those shown outside the lunar orbit were measured by instruments stationed on the moon. The question mark and dashed right-hand segments of some of the component arcs signify that it has not been established whether those components fill the entire upstream region behind their respective foreshock boundaries B, S_e, and S_p, or appear only near these boundaries.

Figure 2. Protons with p = 10 ($E_p \approx 100$ keV) leaving the flank of bow shock within about 4-5° of $\underset{\sim}{B}$ would intersect the lunar orbit at the same point as protons leaving the subsolar region with p = 1.6 (at 50° to $\underset{\sim}{B}$) making it appear that both groups shared the same foreshock boundary at lunar distance.

Figure 3. Schematic representation of field and plasma parameters around and through the bow shock. Field, density, and temperature ratios are scaled vertically in the central sketch for a shock curved with respect to the fixed upstream field $\underset{\sim}{B}_{SW}$, perpendicular at left, parallel at right. The surfaces around the lower part of the figure represent proton distributions in velocity space for various locations with respect to the shock's nonuniform structure.

Figure 4. Schematic electron distributions in velocity space located as in the shock structure diagram of Figure 3.

Figure 5. Schematic profiles of field, particle, and wave behavior through a typical quasi-perpendicular shock crossing. Velocity scales of protons and electrons are independent of each other. In the two wave frequency panels at the top, intensity, indicated by hatching, falls with rising frequency, but spectra may break or peak at plasma or cyclotron frequencies, so the ranges or values of these are indicated by horizontal lines or bars for emphasis.

Figure 6. Conceptual plot of electromagnetic and plasma wave noise levels vs β and M. EM waves are represented by power density at 10 Hz, electric waves by average peak field strength.

Figure 7. Electron drift velocities vs T_e/T_i in shock ramps for four laminar cases. The curves are stability boundaries for ion acoustic waves computed by Manheimer and Boris (A) and Fried and Gould (B).

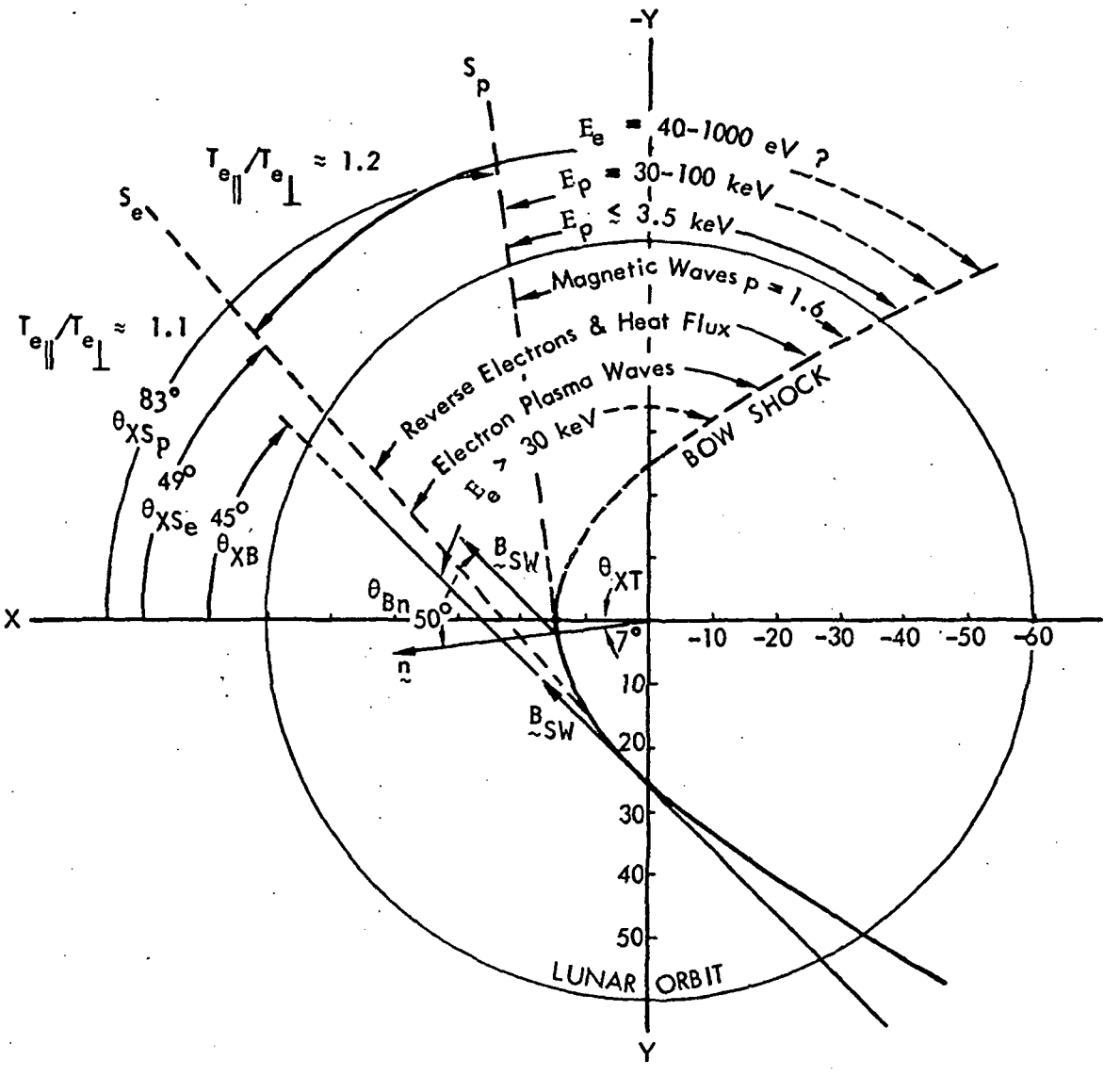

Figure 1. Observed components of the foreshock in an ecliptic plane cross section with the interplanetary field at 45° stream angle. Subscripts e, p refer to electrons and protons. Components shown inside the lunar orbit were discovered by earth satellites, generally at distances up to about 35 R_E; those shown outside the lunar orbit were measured by instruments stationed on the moon. The question mark and dashed right-hand segments of some of the component arcs signify that it has not been established whether those components fill the entire upstream region behind their respective foreshock boundaries, $\underset{\sim}{B}_{SW}$, S_e, and S_p. only near these boundaries.

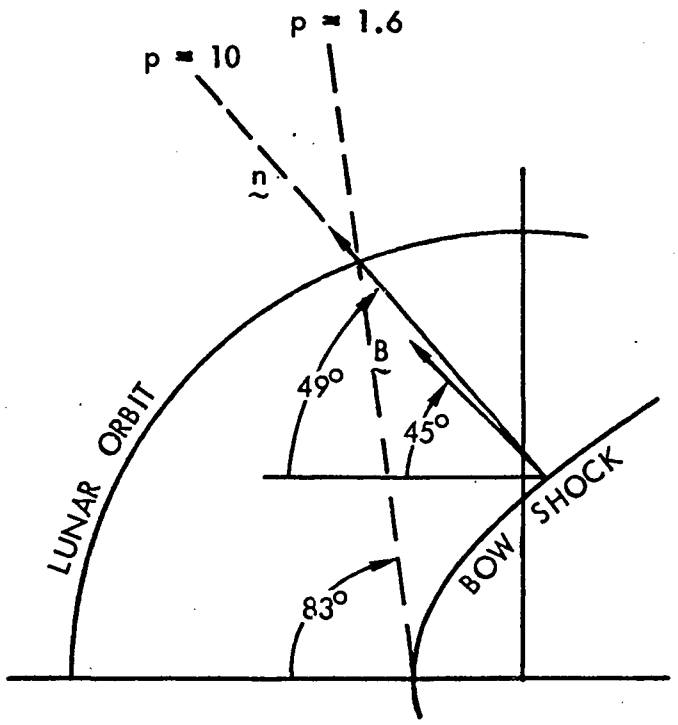

Figure 2. Protons with p = 10 ($E_p \approx 100$ keV) leaving the flank of bow shock within about 4-5° of $\underset{\sim}{B}$ would intersect the lunar orbit at the same point as protons leaving the subsolar region with p = 1.6 (at 50° to $\underset{\sim}{B}$) making it appear that both groups shared the same foreshock boundary at lunar distance.

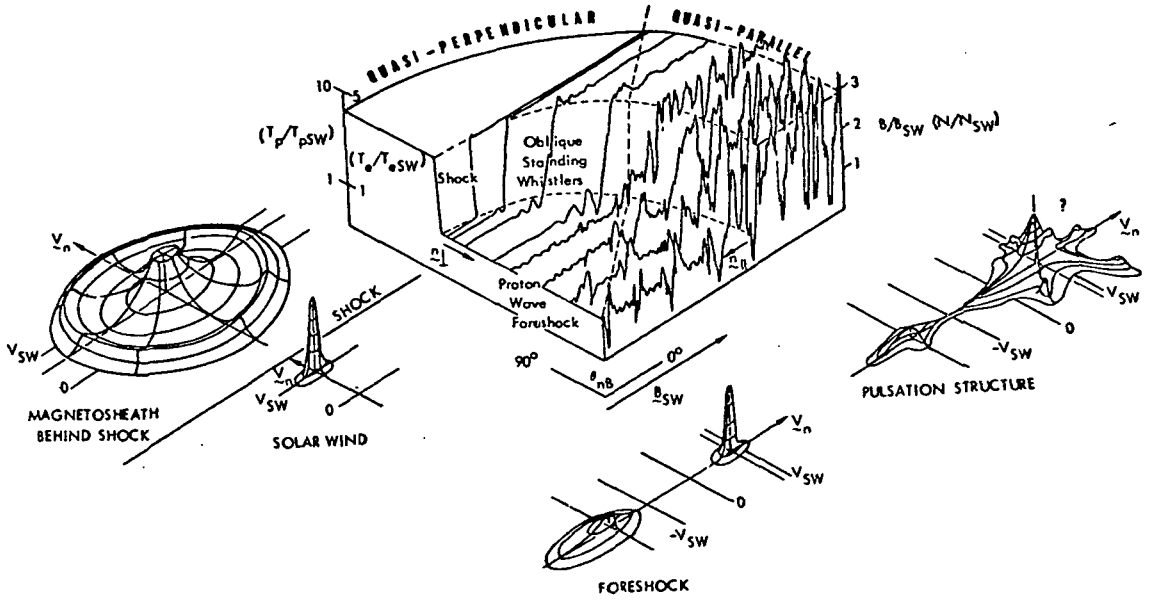

Figure 3. Schematic representation of field and plasma parameters around and through the bow shock. Field, density, and temperature ratios are scaled vertically in the central sketch for a shock curved with respect to the fixed upstream field $\underline{B}_{SW}$, perpendicular at left, parallel at right. The surfaces around the lower part of the figure represent proton distributions in velocity space for various locations with respect to the shock's nonuniform structure.

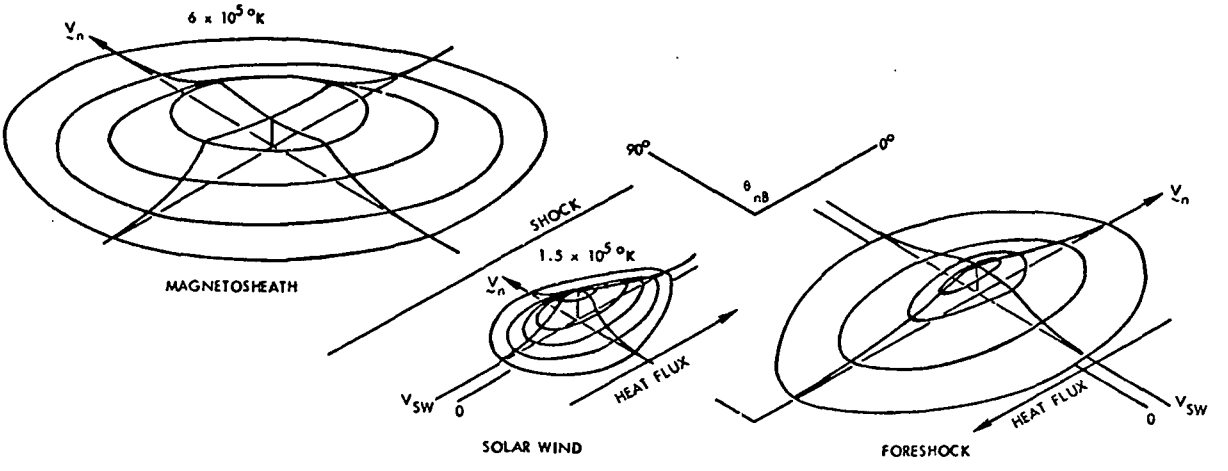

Figure 4. Schematic electron distributions in velocity space located as in the shock structure diagram of Figure 3.

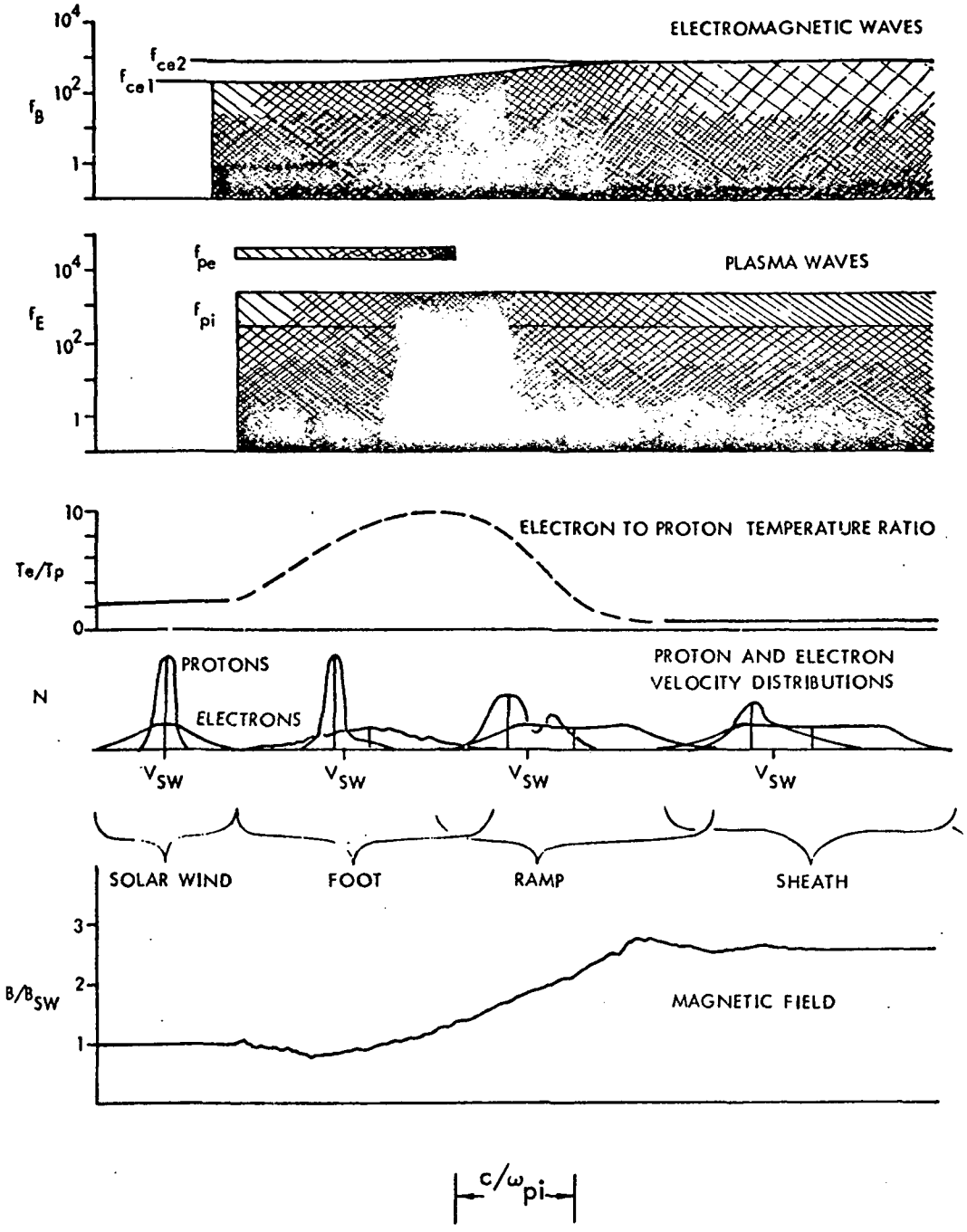

Figure 5. Schematic profiles of field, particle, and wave behavior through a typical quasi-perpendicular shock crossing. Velocity scales of protons and electrons are independent of each other. In the two wave frequency panels at the top, intensity, indicated by hatching, falls with rising frequency, but spectra may break or peak at plasma or cyclotron frequencies, so the ranges or values of these are indicated by horizontal lines or bars for emphasis.

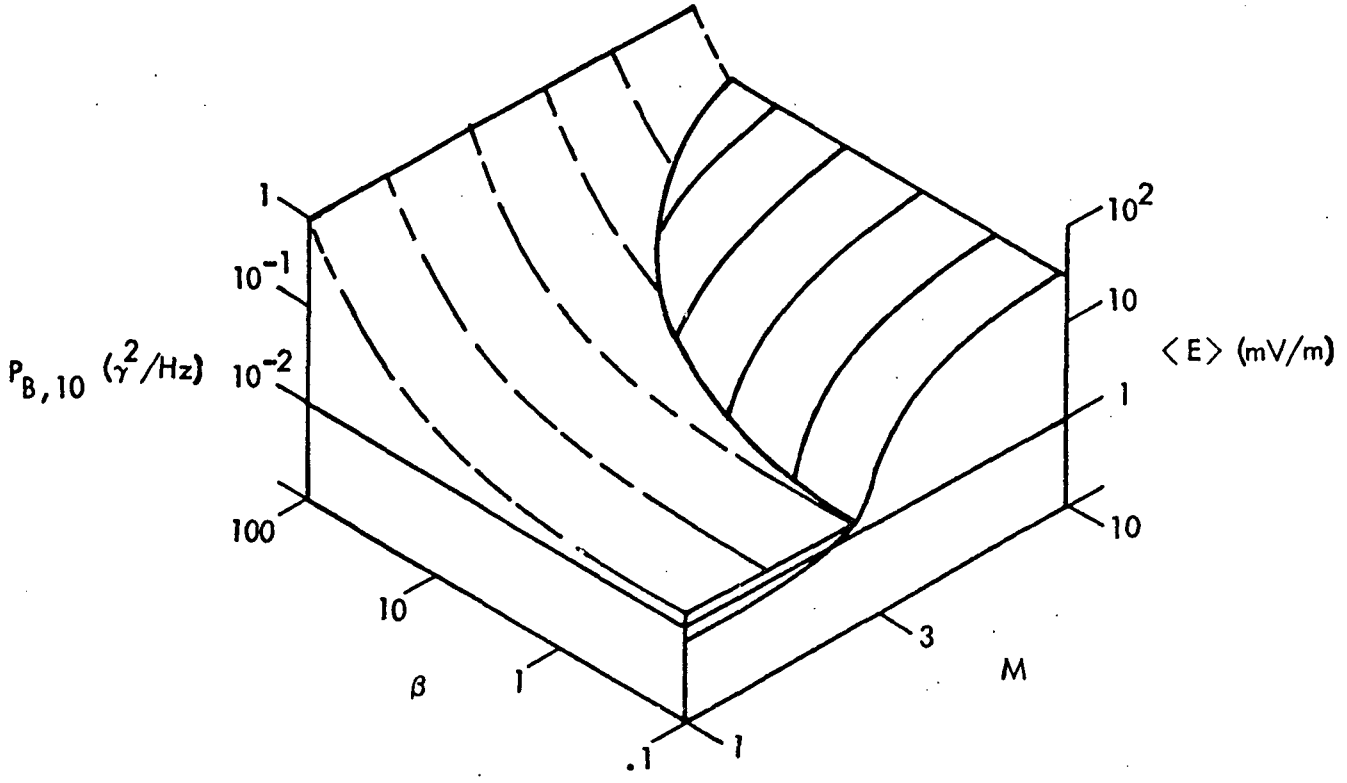

Figure 6. Conceptual plot of electromagnetic and plasma wave noise levels vs β and M. EM waves are represented by power density at 10 Hz, electric waves by average peak field strength.

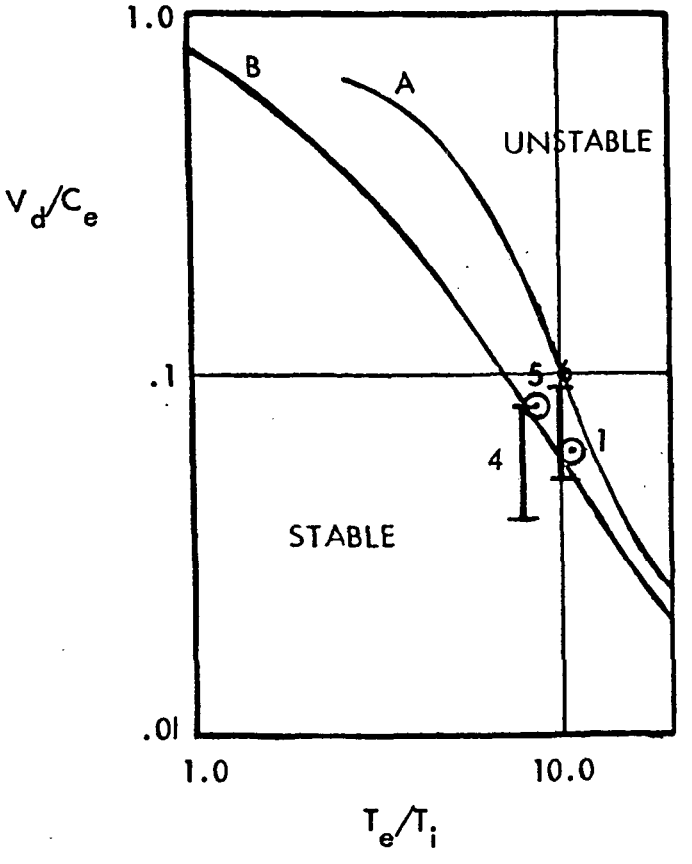

Figure 7. Electron drift velocities vs T_e/T_i in shock ramps for four laminar cases. The curves are stability boundaries for ion acoustic waves computed by Manheimer and Boris (A) and Fried and Gould (B).

APPENDIX B

21333-6017-RU-00

STRUCTURE OF THE QUASI-PARALLEL, QUASI-LAMINAR BOW SHOCK

by

E. W. Greenstadt[1], C. T. Russell[2], V. Formisano[3], P. C. Hedgecock[4], F. L. Scarf[1], M. Neugebauer[5], and R. E. Holzer[2]

May 1975

[1]Space Sciences Department, TRW Systems, One Space Park, Redondo Beach, California 90278

[2]Institute of Geophysics and Planetary Physics, University of California, Los Angeles, Los Angeles, California 90024

[3]CNR-LPS Laboratorio Plasma Spazio, P.O. Box N. 27, 00044 Frascati, Italy

[4]Imperial College of Science and Technology, Department of Physics, South Kensington, London S.W. 7, England

[5]Jet Propulsion Laboratory, 4800 Oak Grove Drive, Pasadena, California 91103

Space Sciences Department

TRW Systems
One Space Park
Redondo Beach, California 90278

STRUCTURE OF THE QUASI-PARALLEL, QUASI-LAMINAR BOW SHOCK

ABSTRACT

A thick, quasi-parallel bow shock structure was observed, for $\theta_{NB} \lesssim 10°$, $\beta_i \approx .3$, $M_A \approx 4$, on 14 February 1969, with field and particle detectors of both HEOS 1 and OGO 5. The typical magnetic pulsation structure was at least 1 to 2 R_e thick radially and was accompanied by irregular but distinct (average) plasma distributions characteristic of neither the solar wind nor the magnetosheath. Waves constituting the large pulsations were polarized principally in the plane of the nominal shock, therefore also in the plane perpendicular to the average interplanetary field. The solar wind was relatively unaffected in bulk velocity in the pulsation structure but was moderately thermalized and its spectra showed a high energy tail. There appeared to be a separate "interpulsation" regime occurring between bursts of large amplitude oscillations. This regime was similar to the upstream wave region magnetically, but was characterized by disturbed plasma flux and enhanced noise around the ion plasma frequency. The shock structure appeared to be largely of an oblique, whistler type, probably complicated by counterstreaming high energy protons. Evidence for firehose instability-based structure was weak at best and probably negative.

INTRODUCTION

One of the fundamental structures of collisionless plasma shocks occurs when the angle θ_{nB} between the magnetic field $\underset{\sim}{B}$ in the unshocked upstream plasma and the direction $\underset{\sim}{n}$ of shock propagation is zero, i.e., when $\theta_{nB} \equiv \arccos(\underset{\sim}{B} \cdot \underset{\sim}{n}/|\underset{\sim}{B}|) = 0$. Such a shock is called a parallel shock and has been studied theoretically and numerically by many authors, of whom a few are Kellogg (1964), Kennel & Sagdeev (1967), Biscamp & Welter (1972), Auer & Völk (1973), and Tidman & Krall (1971). In application to space plasmas, a geometrical basis for variable, asymmetric, and parallel features in the bow shock was postulated very early by Kellogg (1962). Indeed, phenomena probably asscciated with parallel bow shock structure had been the longest recorded, if not the most familiar, shock characteristics since the first penetration of the magnetosheath by Pioneer I in 1958 (Sonett et al., 1959; for a concise summary of the first decade of satellite measurements related to parallel structure see Greenstadt et al, 1970a). Nevertheless, the importance of field orientation to shock phenomenology was not verified observationally or really appreciated until anlaysis of multiple satellite data was undertaken (Greenstadt et al., 1970a, b; Greenstadt, 1972a). Systematic study of these phenomena is the purpose of the investigation described here.

The principal advance in geometric studies since 1970 has been the recognition that a distinct and unmistakable set of macrostructural characteristics occur when $\theta_{nB} \lesssim 40\text{-}50°$, quite unlike the variable, but relatively well-ordered shock signatures that occur in both the laboratory and space when $45° \lesssim \theta_{nB} \leq 90°$ (Robson, 1969; Greenstadt et al., 1975; Fairfield and Feldman, 1975). Shocks with θ_{nB} in the range > 0 to $\approx 45°$, i.e., those having "pulsation"

characteristics and upstream waves, have been designated quasi-parallel. This appellation describes their approximate geometry, their unity of appearance, and their separateness from "quasi-perpendicular" shocks ($45° \lesssim \theta_{nB} < 90°$) while carefully avoiding any implied conclusion that observed features are necessarily identical to those that might be produced under the precise condition $\theta_{nB} = 0$. Theoreticians have generally proposed that phenomena inferred for the $\theta_{nB} = 0$ state could be extended to some $\theta_{nB} \neq 0$, but no firm angular limits to such extrapolations have been determined. In the Discussion section of this paper, we shall question the meaning of exact parallelism in the bow shock, basing our views on the data presented in this communication.

At the same time that geometrically dependent properties of the bow shock have been uncovered, the effects of other parameters of the solar wind plasma on shock structure have also been isolated and investigated. The result has been an empirically-derived scheme of shock classification using β, M, and θ_{nB}, several versions of which have recently been published (Formisano & Hedgecock, 1973a; Formisano, 1974; Greenstadt, 1974). This report is the first account of the quasi-parallel (often to be abbreviated q-parallel) shock in the context of the appropriate thermal and flow parameters of the solar wind, using simultaneous data from three satellites and an array of diagnostics including magnetic and electrostatic plasma wave detectors. The plasma regime represented here differed, but not severely, from the most common one brought to the earth by the solar wind: The mach number and thermal-to-field energy ratio were about 20-30% and 25-50% below average, respectively—not enough to define laminar or cold plasma flow. We deal therefore with a fairly typical, supercritical, warm solar wind. Many macroscopic characteristics of q-parallel structure seem, in our experience, to be common to a wide range of

M, β combinations, but even though the emphasis here is on the character of the shock associated with parallel, or nearly parallel, field geometry, we do not mean to imply that specific features we describe and inferences we discuss apply to any plasma regime other than that (or those) in which the data were recorded.

This paper is one of a series of reports describing the structure of the earth's bow shock in detail for each of several identified combinations of β, M and θ_{nB}. The objective of these reports is to document shock structure from a descriptive point of view, using multiple satellite observations and, insofar as possible, a reasonably uniform set of multiple diagnostics from case-to-case so that comparisons are facilitated and a common foundation for future theoretical analysis and experimental measurements is established. Other communications in the series cover the turbulent shock (Formisano & Hedgecock, 1973b), the laminar, quasi-perpendicular shock (Greenstadt et al, 1975), the high β shock (Formisano et al, 1975a), and the perpendicular shock (Formisano et al., 1975b).

In the following sections we define the category of shock we observed and the measurements from which the data were obtained. We then describe the data in increasing detail and time resolution, alternating between HEOS 1 and OGO 5, and finally discuss and summarize the results.

CATEGORIZATION

There are two major sources of ambiguity in assigning a region of parameter space to a shock such as that described here: one accidental, the other fundamental (assuming perfect instrumentation). Accidental ambiguity arises when no spacecraft is cruising upstream to monitor the true unshocked plasma state. In our case, magnetic, but no plasma, data were available, except for a few scattered samples during brief quiet intervals which, by their very nature, may not have corresponded to the unquiet structure under scrutiny. Fundamental ambiguity arises when the highly irregular and noisy quasi-parallel structure makes the application of even the best upstream measurements problematical: there may be no well-defined "normal" with which to determine the local field-normal angle θ_{nB}, and the extensive upstream effects of the structure may modify the oncoming solar wind so much that velocities, temperatures, temperature ratios and anisotropies, and densities at what we might prefer to call the actual "shock" bear little resemblance to their distant upstream counterparts.

In our case there were some short periods close to or within the interval of interest whose measurements by one or the other satellite we simply took to be the best available representation of the background solar wind plasma. From these measurements we obtained the estimates: $\beta_i = 8\pi NkT_i/B^2 \approx .3$; $\beta_{total} \doteq 8\pi Nk(T_i t^+ T_e)/B^2 \approx .6$; $M_A = V_{SW} \cos \theta_{Xn}/C_A \approx 3.7$ and 4.2; $M_{MS} = V_{SW} \cos \theta_{Xn}/(C_A^2+C_S^2)^{1/2} \approx 3.4$ and 3.9, where $C_A = B/(4\pi Nm_i)^{1/2}$, $C_S = (kT_e/m_i)^{1/2}$, and we have assumed $T_e = 1.5 \times 10^{5}$°K. The double estimates of Alfvén and magnetosonic mach numbers apply to the positions of HEOS and OGO, which had slightly differing nominal angles $\theta_{Xn} \approx 32°$ and $42°$, between solar wind flow and the local shock normals; the first of each pair refers to HEOS 1.

The values estimated place the shock in a category between quasi-laminar and turbulent, according to the scheme of Formisano and Hedgecock (1973a; see also Greenstadt, 1974), because it was supercritical ($M_A \gtrsim 3$), with $\beta_i \lesssim 1$, on the basis of imputed upstream plasma conditions. We reiterate that within the structure, conditions may have differed, probably raising β and lowering M moderately. The mach number might conceivably have become subcritical in the shock structure, and the category have shifted to quasi-turbulent; i.e., $M_A \lesssim 3$, $\beta_i \gtrsim 1$ (Formisano and Hedgecock, 1973a).

The important field-normal angle θ_{nB} was the best-determined parameter upstream (from independent observation by a third satellite) but nonetheless poorly-determined locally, since the field, and presumably the shock "surface," were highly variable. Data could be cited which would reasonably have put θ_{nB} in the range 0 to 20°. Our best overall estimate is $\theta_{nB} \approx 4$ to 10°, so we have placed the shock in the quasi-parallel category, carefully avoiding commitment to the virtually undocumentable term "parallel shock." We emphasize, however, that θ_{nB} was close to zero and that we deal here with borderline parallel geometry.

MEASUREMENTS

The data shown here were obtained by the TRW plasma wave detector of OGO 5, the triaxial fluxgate magnetometers of OGO 5 (UCLA) and HEOS 1 (Imperial College), and the JPL plasma analyzer, Lockheed light ion spectrometer (LIS), and UCLA/JPL search coils of OGO 5. The OGO 5 instruments provided high resolution records of the shock at sampling intervals of 1.15 sec/sample, corresponding to a 1 kilobit/sec telemetry rate.

The field and particle instrumentation of OGO 5 and HEOS 1 that provided data for this report are described by Bonetti et al. (1969), Hedgecock (1975), Crook et al. (1969), Snare and Benjamin (1966), Harris and Sharp (1969), and Neugebauer (1970). In using data from the Lockheed spectrometer, we rely here only on relative changes in the raw signature of its energy sweep.

Magnetic field measurements are direct vector recordings of ambient induction, with the HEOS 1 data used to adjust the absolute bias levels of the OGO 5 readings, the latter having been subject to intermittent spacecraft interference. Plasma wave measurements were represented by the field strength in seven channels covering the range 1 to 70 kHz, with most of the shock noise contributed by signals between a few hundred Hz and 2 kHz. Channel center frequencies were at .56, 1.3, 3, 7.35, 14.5, 30, and 70 kHz. Electromagnetic wave noise is represented by the equivalent level of white noise over the bandwidth of each of seven channels of the UCLA/JPL search coils, with center frequencies at 10, 22, 47, 100, 220, 410, and 999 Hz. The JPL plasma analyzer provided plasma flux readings and upstream velocity and density parameters in the solar wind. The plasma flux was measured by the JPL Faraday Cup, which maintained a fixed view toward the sun, with acceptance angle determined by

50 percent transmission at 20° and zero near 40°; absence or decrease of flux usually signifies deflection of flow outside the acceptance angle of the instrument. These quantities were therefore lost once OGO entered the normal sheath. Proton thermalization and diversion of solar wind protons in directions away from that of normal flow were detected by the Lockheed LIS, after the shock was entered, since this instrument looked only in a direction across the solar wind stream. These last measurements are represented here by relative changes in uncalibrated telemetry units.

In addition to the data illustrated in this report, plasma and magnetic field parameters for the unshocked solar wind were obtained from the magnetometer of Explorer 35 (NASA/ARC).

MAGNETIC PROFILE

An overall view of the phenomena of 14 February described in this report is furnished by Figure 1. The two major panels show the field magnitudes measured by HEOS 1 and OGO 5 magnetometers; one-minute averages in the case of OGO and 48-second samples in the case of HEOS. The three narrow panels at the top show the magnitude and two angles of the interplanetary field $\underset{\sim}{B}_{SW}$ recorded concurrently near the moon by Explorer 35; these are 82-second averages. Note the steadiness of $\underset{\sim}{B}_{SW}$ in contrast with the violent swings in B at the two earth satellites. Indeed, even the direction of $\underset{\sim}{B}_{SW}$ was less variable for this study interval than it usually is.

The two inserts labelled I_p show the behavior of the "binary index" (Greenstadt, 1972b) at the positions of OGO and HEOS, calculated from the field directions measured by Explorer. Values 1 and 0, respectively, are supposed to correpond to q-parallel and q-perpendicular field orientations. We see that shifts between the two levels correspond to changes in orientation of B_{SW} and that the obvious encounters with pulsation shock conditions at both spacecraft occurred while $I_p = 1$. There was a delay for travel time between Explorer and the other vehicles which may have varied during the day; at 0630 it seems to have been about 15 minutes, with the switch from $I_p = 1$ to $I_p = 0$ matching a brief disappearance of upstream waves at OGO and HEOS a short time later. The index is presumably applicable at a given instant only strictly at the "shock," the location of which is unknown almost all of the time, and which appears to be altogether fictitious when the field is locally quasi-parallel.

The numbered times of Figure 1 call attention to specific events: 1., the first, q-perpendicular crossing by OGO 5; 2., the sudden onset of large

amplitude fluctuations at HEOS 1, obviously a downstream pulsation limit at that instant; 3., the sudden onset of large amplitude fluctuations at OGO, clearly an upstream pulsation limit at that instant, since OGO had already been in the solar wind; 4., the cessation of pulsations and second appearance of solar wind at OGO; 5., the first appearance of solar wind at HEOS. These events will be mentioned in the next section.

GEOMETRIC CONFIGURATION AND SHOCK THICKNESS

The relative positions of spacecraft and shock are illustrated in Figure 2. The first panel, (a) at upper left, displays the trajectory segments of HEOS 1 and OGO 5 appropriate to the shock observations of Figure 1, together with sections of shock curves corresponding to the previously-numbered events. The satellite positions and shock curves are depicted in the rotationally-symmetric X-ρ frame, where $\rho^2 = Y^2 + Z^2$, and shock sections are drawn by simple scale multiplication of the surface $\rho^2 = .331\ [(X - 75.25)^2 - 3686)]$. This surface is a symmetrized version of the average shock described by Fairfield (1971). Both spacecraft were moving outward along their respective orbits during the data interval. The heavy portions of the segments represent the pulsation observations.

Figure 2(a) shows the limits on shock location implied by the data of Figure 1: at time 1, the shock was actually at OGO 5, after which it contracted, but moved no closer to the earth than the location of HEOS 1, which was clearly in the magnetosheath at least until time 2, when large amplitude pulsations were first recorded. The brief, unnumbered rise in B at OGO just after 0300 (Figure 1) was a shock encounter which ended at 0314, just five minutes before pulsations began at HEOS (time 2), so the shock was definitely at OGO at that time. At time 2, the shock, or, preferably, the innermost unshocked solar wind was somewhere outside HEOS and inside OGO, the former being in the pulsation region, and in the latter in the upstream wave region. At time 3, the outer boundary of the pulsation region moved outward beyond OGO. After time 4, OGO was again in the solar wind, but the shock was still outside of

HEOS until time 5, when the shock finally moved inside of HEOS, leaving both satellites in the upstream wave region in the solar wind.

Figure 2(b) shows the satellite positions projected on the Y-Z plane (X=0), as viewed looking from the sun toward the earth. The two spacecraft were within 12° of occupying a common plane through the X-axis.

It is immediately apparent from Figures 1 and 2(a) that during the simultaneous observations of the large amplitude pulsations, between times 3 and 4, the two satellites did not occupy the same nominal symmetric shock surface. It would follow that the thin shock had been replaced by a "thick pulsation region." An objection could be raised that taking into account aberrational asymmetry of the shock caused by nonradial solar wind flow might place the vehicles on the same nominal shock surface. The pulsations could then have been some sort of surface wave phenomenon and not a thick region at all. Figure 2(c) shows two curves representing the nominal shock symmetric about an axis, but tipped away from the X-axis as if in a common plane containing both spacecraft. The 15° tilt of the shock brings the two satellite positions closer to lying on the same shock surface than does any other tilt angle, but the vehicles are still separated radially by about .5-1 R_e. Thus, the concept of a thickened pulsation shock cannot be dismissed by substituting simple coordinate rotation. Moreover, a 15° solar wind aberration conveniently northward in the general direction of the two spacecraft for over an hour would have been extraordinary in every way. The most reasonable conclusion is that these data confirm the earlier observations and support the postulate of a thick pulsation region developing under parallel, or quasi-parallel, conditions (Greenstadt et al., 1970a).

In Figure 2(d) we return to the unaberrated, nominal shock profile to derive a lower limit of the possible thickness of the quasi-parallel shock. The two curve segments marked 3 correspond to the beginning of the common part of the pulsation interval at the respective vehicles; the segments 4 correspond to the end of the common interval. The minimal thickness of the quasi-parallel structure, as provided in this configuration by distances 3-3 or 4-4 along the local nominal shock normal, are estimated to have been 2 to 2.5 R_e, depending on how far from the subsolar point the thickness is taken.

The evidence supports the attribution of an appreciable *minimum* thickness to the q-parallel shock structure, but does not supply a basis for estimating a *maximum* thickness (other than from the magnetosphere to the spacecraft at time 4, say). Returning to Figure 1, however, we note that following time 4, pulsations persisted at HEOS although they had been replaced at OGO by upstream waves and that following time 5, upstream waves continued, with short, scattered breaks, for many hours at both satellites, with almost constant amplitude. We are led to the tentative conclusion that for a given field orientation, an equilibrium configuration is established in which a pulsation boundary, like the upstream wave boundary, is created. The distance of the pulsation boundary may maximize along $\underset{\sim}{B}_{SW}$ in the solar wind frame.

PLASMA PROFILE

HEOS 1

The HEOS plasma data afford a view of the general effect of the quasi-parallel shock structure on the solar wind. Figure 3 compares the magnetic profile of the 14 February shock with the plasma parameters derived from the processing scheme of the HEOS 1 plasma analyzer (Bonetti et al., 1969; Formisano et al., 1973). Estimated plasma quantities are, from the top, thermal velocity w, distribution skewness-measure K, density N, and velocity V. Infinite K means a Maxwellian energy distribution; lower K indicates a high-energy tail, at least for a smooth and regular, but skewed, distribution function (Formisano et al., 1973). Each (vertical) set of plasma quantities represents the ensemble of values computed from a single, complete, 384-sec cycle of the analyzer spanning the corresponding time segment.

The behavior of the bulk velocity V is the most remarkable, because it is the least striking, of the plasma parameters. Scanning from right to left, in the direction traveled by the solar wind to the magnetosphere, we see that, except for a sharp dip in V during a single spectral cycle at about 0520, the encounter of the solar wind with the high fields and high-amplitude pulsations of the outer part of the quasi-parallel "shock" is virtually undistinguishable in the velocity graph. The circled points represent a few velocities observed concurrently by OGO 5, showing the relative constancy of V during the interval and the excellent agreement between the instruments. Only after appreciable penetration of the "shock," at about 0440, did V decrease for more than one cycle at a time, and only after magnetosheath conditions were clearly established

magnetically, at about 0315, did V experience a sharp "permanent" decrease. Moreover, inspection of the individual cycles in the structure (described in a later paragraph) reveals no simple downward shifts in bulk velocity between and 0400-0500, but irregular, multimodal spectral distributions whose highest peaks were near the solar wind bulk velocity.

The single drop in V at 0520, which corresponded to a sudden spike in B, is probably attributable to a brief encounter with the shock in quasi-perpendicular form. The OGO field data show simultaneously some average direction changes and some brief disappearances of upstream waves suggestive of local changes in obliquity. Unfortunately, the Explorer 35 record suffered a data gap at that time (Figure 1).

In contrast to the velocity, the remaining plasma parameters display clear differences between pulsation and upstream values, requiring very careful examination. Note that the instants of initiation of change are not clearly all the same for w, K and N and that these computer-derived parameters were more or less artificially constructed, anyway, depending on the particular cycle. These quantities suggest, on balance, a rise in w (temperature) and N and a non-Maxwellian skewing of the ion distribution toward higher energies in the quasi-parallel structure, compared to the solar wind. However, some variation evidently also occurred in the undisturbed solar wind, although there were no independent data with which to evaluate this possibility. The dashed vertical line marks what we believe was a density discontinuity in the solar wind. This decrease in N occurred a few minutes after the last large field gradient, so it was probably unrelated to the shock structure. The four circled points earlier in the graph, just after

spectra obtained by HEOS 1 respectively before 0315 and after 0520 (only when upstream waves were absent in this case). By "average" it is meant that the counts in each energy channel were averaged among the several cycles. Individual spectra contributing to either magnetosheath or solar wind averages were comparatively repetitive and differed little from their corresponding means. The distribution marked "pulsation region" is the average, in the foregoing sense, of all cycles obtained during the two hours or so of pulsation field profile at HEOS. This spectrum clearly shows the plasma energy peak at, or slightly below, the bulk energy of the solar wind but with a lower maximum and a broadened, hotter, more skewed ion distribution. It appears that the ions were severely scattered but the flow was not appreciably retarded by the large amplitude magnetic waves of the parallel structure. This is the same story told by w, K, and V in Figure 3.

Figure 4(b) demonstrates that the distinction just made between the three curves in 4(a) is not an artifact of the averaging process. The three solid curves in 4(b) represent the highest, lowest, and average readings of each energy channel, for all the pulsation spectra. The upper dashed curve is a composite representing for each channel, the highest of either solar wind or magnetosheath readings for that channel in any of the selected spectra used for the sheath and wind averages in 4(a). The lower dashed curve represents the lowest of either magnetosheath or solar wind readings in each channel among the same spectra. We see, first, that the average pulsation ion spectrum was reasonably representative of the pulsation extremes, and, second, that the envelope, and even the average, of the pulsation ion spectra was not contained within the envelope of the composite distributions. Thus the ion

distributions in the quasi-parallel structure appear to have formed a distinct class of spectra separate from those of either the magnetosheath or the solar wind. This distinction will be elaborated further in the high-resolution section.

For the sake of completeness, Figure 4(c) displays two extremes of the individual pulsation distributions showing two traits typical of all of them: the irregularity below the bulk velocity and the filling-in of the dip between proton and alpha peaks of the solar wind distributions. Most individual distributions resembled either of these or a composite of them.

OGO 5

The upper panels of Figure 5(a) compare the time history of the solar wind flux, when measured by the JPL Faraday cup, with the field magnitude recorded by the UCLA fluxgates. The plotted points are 1-minute averages. Gaps in the flux represent alternate modes of instrument operation. The graphs show the extremely erratic nature of the flux, along with the field, in the quasi-parallel structure between 0350 and 0510. The vertical bars call attention to the apparent inverse relation of F and B: when one is high, the other is correspondingly low.

The lower box, Figure 5(b), is a scatter plot of F against B for the interval 0355-0512. The bars define the high, low, and midrange values of F for each 1γ interval of B. The approximately inverse relationship between the quantities is clear for values of B ranging between solar wind and magnetosheath levels. The curve in Figure 5(b) is a visual fit of the simple inverse expression $F = 925/B$.

The direction of the solar wind flow at OGO was, like the flux itself, highly erratic between 0355 and 0512, and we know from the HEOS data (preceding description) and from occasional measurements of V_{SW} at OGO, that the velocity was not radically altered in the q-parallel structure. We also know that density often rose in the structure at HEOS. The irregular flux profile, especially the minima in flux, were therefore not produced by variations in V or N but by deflections of the solar wind flow and possibly also by scattering of some of the particle distribution outside the acceptance angles of the instrument (partial transverse thermalization) so that N_X, the density in the view direction, would have been reduced even for zero wind deflection when pulsations were present upwind from the satellite. Such scattering would be consistent with the observed average distributions at HEOS already described.

HIGH RESOLUTION DATA

HEOS 1

The averaged plasma distributions already illustrated serve to demonstrate the existence of a separate category of ion spectra associated with the bow shock's quasi-parallel magnetic profile. They are poor guides, however, to the instantaneous appearance of the plasma over time intervals less than or on the order of a single sampling cycle. The typical period, i.e., peak-to-peak time-interval, of the most conspicuous field fluctuations was near ten seconds, appreciably less than the total HEOS plasma probe cycling time of 384 seconds. Thus, in many cases, individual spectra could not have represented stationary plasma properties.

This aliasing of plasma spectra was anticipated in design of the HEOS 1 analyzer, so that each energy cycle was divided into four 96-second cycles, each of which covered a wide energy range by sampling every fourth channel. The subcycle feature of the instrument has already been described and used to advantage in an earlier paper (Formisano and Hedgecock, 1973b). In the present report, the subcycle representation of the ion distributions is the only acceptable way of portraying the plasma behavior at high resolution within the pulsation structure at HEOS. It must be remembered, however, that the 96-second subcycle period was also too long to allow accurate depiction of the transient ion distributions in most cases.

The record of field magnitude at HEOS 1 between 0300 and 0600 is shown at the top of Figure 6. Segments of the interval corresponding to representative ion spectral sampling cycles are marked by the lettered and numbered

boxes. The energy distributions of the selected cycles are shown below, with the four component subcycles of each cycle displayed approximately in the actual time sequence in which they were acquired. The two spectra inserted at lower right are average solar wind and magnetosheath distributions. These are repeated in each cycle for comparison with the data actually obtained during the selected cycle. Points at the sampled energies within each subcycle are joined by straight lines.

Cycle A1 occurred entirely in the magnetosheath, apparently when I_p = 0 (Figure 1). The distribution is virtually indistinguishable from that of the average magnetosheath. This example illustrates how steady and reproducible the magnetosheath ion spectrum can be under $I_p = 0$ (quasi-perpendicular) conditions. Cycle A2 spanned a change in plasma regime. The first two subcycles were close to the magnetosheath pattern, while the last two subcycles were a mixture of modified solar wind and magnetosheath patterns. There is no way of knowing in this case whether the sudden transition and drop in field was attributable to crossing of a stationary, or semistationary, boundary between steady magnetosheath and pulsation shock structure or to an encounter with newly-excited pulsation, i.e., quasi-parallel, structure propagating back through the sheath. We are inclined, because of the change of I_p from 0 to 1 at about that time, to favor the latter explanation. Cycle A3 was clearly neither magnetosheath nor solar wind, although there was a strong solar wind contribution during the third subcycle. This feature is particularly noteworthy since the high field magnitudes simultaneous with the last half of cycle A3 would seem to have made the presence of solar wind characteristics least probable at that time.

Cycle B, in the midst of the quasi-parallel shock, began during low field readings and ended during high field readings. The distribution, however, was clearly not a simple composite of sheath and wind subcycles. The spectrum was characteristic of neither of these two relatively stationary regimes.

Cycles C1 and 2, also in the midst of the quasi-parallel shock, were likewise neither sheath nor wind. Careful examination of cycles B, C1, and C2 will show that these three distributions were generally similar to each other, despite the rather extreme variations of the field that took place during their acquisition.

Cycle D, still in the pulsation structure, demonstrates the variability of the spectra found there. Again, the distribution was neither sheath nor wind.

Cycle E spanned the change from shock to solar wind. The first two subcycles were very irregular, the third was almost exactly like the solar wind, and the last was evidently representative of the shock structure, as in Cycles B and D, despite low concurrent field magnitudes.

The last illustrated distribution, Cycle F, exhibited the type of modification common to solar and spectra in the presence of upstream waves. The distribution was basically that of the solar wind, with some deviations, particularly in the second subcycle. Recall that the average solar wind spectrum was derived from intervals in which upstream waves were absent.

To summarize the behavior of the plasma ions (protons), on the finest time scale available to the HEOS 1 detector, the particle energy distributions

were irregular and variable within the quasi-parallel shock structure. Nevertheless, a certain similarity among proton spectra was apparent, even when separated from each other in time. These pulsation-associated spectra were definitely not mere time-aliased composites of regular magnetosheath and solar wind distributions.

OGO 5

Wave Polarization. The OGO fluxgate data were transformed into a frame in which the Z-axis contained the least jump during the interval surrounding the abrupt, q-perpendicular shock crossing of 0251 (Figures 1, 8(a)). Thus, the Z-component should be aligned approximately with the nominal local shock normal. The X-axis was then selected to coincide as closely as possible with the $\underset{\sim}{B}$-vector component in the shock (X-Y) plane. Figure 7 illustrates two sections of field-component data, one in the sheath behind the Q-perpendicular shock, the other in the midst of the Q-parallel structure. The general context of these sections can be seen by reference to Figure 5. We see that most of the small amplitude fluctuation in the sheath was in the Y-Z plane, and that most of the large amplitude fluctuation of the shock was in the X-Y plane. Both sets of oscillations were therefore composed of transverse waves propagating more or less parallel to $\underset{\sim}{B}$, for in the q-parallel structure $\underset{\sim}{B}$ had rotated so as to be nearly parallel to the nominal normal, i.e., the Z-axis. The amplitude of the Z-component in the shock is by no means negligible, a circumstance compatible with poorly-defined $\underset{\sim}{\overline{B}}$ and $\underset{\sim}{n}$ when $\Delta B/B$ is so large.

Multiple Diagnostics. Figures 8(a) thru (e) display a number of sections of data as viewed simultaneously by both particle and field instruments of

OGO 5. The sections were chosen to illustrate the full range of forms visible in the OGO record. These are: Figure 8(a), the abrupt, quasi-perpendicular crossing of 0251; Figure 8(b), a gradual transition from high to low average (apparently solar wind) field readings; Figure 8(c), two examples, (i), (iv), of upstream waves directly connected to definite, undisturbed solar wind and two examples, (ii), (iii), of similar waves occurring between sections of pulsations; Figure 8(d), two relatively brief bursts of large amplitude pulsations; and Figure 8(e), two prolonged sojourns in the pulsation structure. In Figures 8(b)-(e), the magnetic X-axis is included to represent typical component behavior of the field in the nominal "shock plane."

The abrupt jump from "quiet" magnetosheath to "quiet" solar wind is shown in Figure 8(a) as a reference with which to compare the less familiar quasi-parallel forms of subsequent figures. With the exception of B_X, omitted in (a), the panels are the same for the other figures, (b)-(e). These are, bottom to top: magnitude of B; plasma wave electric noise as sampled sequentially in seven passband channels; proton appearance (in telemetry units), as seen in a direction across the nominal solar wind flow, hence indicating a combination of deflection and thermalization; solar wind proton flux as seen looking toward the sun into the nominal, undeflected solar wind; VLF magnetic noise and sampled by seven channels along one axis of the OGO search coil magnetometer. At the left of the plasma wave panel a typical solar wind spectral signature has been superposed (dotted lines) to mark the contrast between quiet upstream and downstream spectra surrounding a familiar quasi-perpendicular shock crossing; note that the three lowest frequency channels register enhanced noise in the sheath. In the uppermost panel, the measurements of selected

ELF channels have been calibrated and plotted on a common vertical scale, so the relative values seen by various channels can be readily intercompared. Thus a significant enhancement of one channel with respect to the ones adjacent indicates a significant departure from a simple falling spectrum, probably implying the appearance of an ambient signal near centerband of the affected channel. Channel selection from figure to figure represented a compromise between showing important ELF effects and avoiding the confusion of too many overlapping curves.

Several features of Figure 8 are important. First, there were sudden changes in average solar wind flux at the shock and in the deflection of protons into the Lockheed instrument. Second, the deflection of particles detected by the LIS was essentially continuous although not constant, in the sheath. Third, thermalization of the protons clearly occurred just behind the ramp. Fourth, the magnetic noise peaked around the shock for all channels with $f \leq 216$ Hz, but showed behavior upstream substantially identical to that downstream, with the most active channel centered at 100 Hz. Although this shock was supercritical and not laminar, the ELF noise followed the same whistler mode pattern seen in the laminar shock (Greenstadt et al., 1975). The large relative separation between the 100 Hz and 216 Hz noise levels resulted from the whistler cutoff at the electron cyclotron frequency along the shock normal. The frequency f_{ci} was about 220 Hz ($B \approx 8$) in front of the shock and 530 Hz ($B \simeq 19\gamma$) behind it, but since θ_{nB} was about 60° in front and 77° behind, $f_{ci} \cos \theta_{nB}$ was approximately 110 Hz both upstream and downstream. As Figure 8 shows, frequencies $f < 100$ Hz were enhanced just outside and frequencies $100 \lesssim f \lesssim 216$ Hz just inside the shock, corresponding to detection of rapidly-damped, shock-generated whistlers below the rising f_{ci} in the B-gradient. A more detailed exposition of the ELF phenomenon can be found in the reference cited above.

The contrast between Figures 8(a) and (b) is of considerable interest. Seen by itself, the magnetic field, particularly its magnitude profile (2nd panel from the bottom), suggests a "gradual" shock crossing in which the mean field dropped from about 20γ at far left to 10γ or less by 0439, the latter value being close to the interplanetary field. But no other diagnostic supported this view. The solar wind flux, for one, did not return to an average upstream value when the field had been reduced, but showed violent fluctuations including very low flux levels characteristic of the steady magnetosheath (Figure 8(a)). The plasma wave spectrum did not reproduce its typical solar wind format, and the ELF magnetic noise channels showed appreciably more activity at the lower frequencies than they had either in the sheath or the solar wind surrounding the abrupt crossing of Figure 8(a). Conversely, the steady deflection or thermalization of protons associated with the sheath in Figure 8(a) did not appear when B was up to sheath level at 0434. This last observation can be strengthened by reference to Figure 8(e)(ii), which continues Figure 8(b) (to the left): there were nearly two minutes of relatively high average field in which significant thermalization was not apparent. Note that the relatively high and steady field segment surrounding 0438 was accompanied by relatively elevated flux and no evident thermalization. In sum, the quasi-parallel transition from high to low field was grossly different from the quasi-perpendicular case.

The foregoing description leads directly to disclosure of a wholly new phenomenon which for purposes of this report we designate the "interpulsation regime." In an early report on the "pulsation shock" (Greenstadt et al., 1970a,b), attention was called to the appearance of bursts of large amplitude

oscillation, separated by "upstream waves," which appeared almost periodically in the data. The same type of periodic-burst feature occurred in part of the interval we analyze here, but now we are compelled to drop the notion that the bursts are separated by upstream waves. Figure 8(c) depicts two examples of genuine upstream waves (i) and (iv), and two examples of interpulsation waves, (ii) and (iii). The mean field magnitude in all four cases is almost the same, and essentially at the interplanetary field level, while the character of the waves is at least superficially indistinguishable in the magnitude panels. There is a hint of higher frequencies and perhaps slightly larger amplitudes present in (ii) and (iii) than in (i) and (iv), but only by contrast. A distinction between the pairs appears readily, however, in the other diagnostics.

Unfortunately, OGO solar wind flux measurements were not available for the two solar wind segments (see Figure 5(a)), which were selected independently for other reasons: both represented upstream wave trains connected directly to undisturbed interplanetary field, either before or after the waves. The first, in panel c(i), was chosen because it occurred after twenty minutes of upstream waves following a brief exposure to clean solar wind and shortly before the appearance of large amplitude oscillations. Thus this segment should be "deep" in the upstream wave region, near the "shock." The fourth, in panel c(iv), was chosen because the waves were at the edge of the upstream wave region, obviously connected immediately to unperturbed solar wind, as the figure shows. We emphasize that all four of the examples of 8(c) were within the "band" of solar wind we postulated might have been bounded by density discontinuities around 0315 and 0550.

The flux is included in panels c(ii),(iii) for completeness, but little can be inferred from it since it is absent from (i) and (iv). We note that

the levels are rather low, but it is possible that the incoming solar wind flux may have varied somewhat over the total half day we are examining, and within any subinterval. Nevertheless, there are extremely low values in (iii) that are hardly compatible with the apparent interplanetary field level they accompany.

Of more interest are the Lockheed data in the fourth panel from the bottom in all four segments. There was no activity above background in (i) or (iv), nor indeed was there such activity at any time during the almost six hours of unambiguous upstream wave residence by OGO on 14 February. Moreover, there is no visible change in the Lockheed record after 0516 in (iv), leaving perturbed and unperturbed sections indistinguishable. In (iii), on the other hand, there was a trace of activity at about the center of the segment, while in (ii) small readings of proton deflection and/or thermalization were constantly present. This type of low level, intermittent "cross-flow" proton noise was characteristic of interpulsation segments.

The wave measurements confirm the proton data. The three plasma wave spectra in (i) and (iv) are typical of the solar wind. In fact, no significant alteration of the spectra pattern occurred after the onset of upstream waves in (iv). In contrast, the spectrum of (ii) was moderately altered, particularly in the 1.3 kHz channel, while the spectrum of (iii) departed radically from the solar wind form in the two lowest frequency channels. Similarly, magnetic noise differed between the two pairs of segments: the average noise levels at the lowest frequencies were slightly higher in at least part of the (ii) segment than in either solar wind example, while the ELF noise in (iii) was decidedly enhanced over that in any of the other examples.

To summarize, true solar wind data were similar to each other whether representative of unperturbed solar wind, upstream wave onset, or "deep" upstream wave observation, while interpulsation waves, appearing to emulate upstream waves magnetically, showed diagnostic features suggestive of a quite different regime.

The remaining pair of this group of examples, Figures 8(d) and (e), display the large pulsations themselves, which are the essence of the quasi-parallel structure. Figure 8(d) shows two short bursts of pulsations; Figure 8(e) shows two data segments out of longer intervals of continuous pulsations.

The quasi-periodic character of the large oscillations is striking, particularly in the components, as the illustrated B_X shows. The full array of diagnostics demonstrates that the pulsation profiles were neither solar wind nor magnetosheath nor alternating samples of these two regimes. The deflection and/or thermalization of the solar wind stream was evident in both the JPL and Lockheed data when the "megapulsations" were present: the flux stream diminished, fluctuated, and almost disappeared, while protons appeared irregularly across the normal flow in the light ion spectrometer. Electric plasma wave and magnetic ELF wave noise levels were enhanced to values higher than those sustained in the sheath and were comparable to those normally associated with low β, low M, quasi-perpendicular shock crossings. The examples Figure 8(d) substantiate the distinction in Figure 8(c) between upstream and interpulsation wave regimes by exhibiting, particularly in the ELF wave measurements of 8(d)(ii), little distinction between burst and adjacent data.

DISCUSSION

Magnetic Structure

The distinct character of the pulsation structure of the q-parallel shock has been seen in both magnetic and plasma diagnostics, and the geometry of dual satellite observations here and in an earlier study (Greenstadt et al., 1970a) have implied that the pulsation region can be quite thick. The accidentally similar radial placement of the pairs of satellites in both studies have confirmed the minimal thickness of $\approx 2\ R_E$, but prevented the estimation of any upper limit to the thickness. One additional item is valuable in demonstrating the nature of the extended region occupied by this structure. Figure 9 displays, in a common panel, the sections of pulsation structure recorded simultaneously by OGO 5 and HEOS 1 magnetometers. In this figure, the OGO field measurements have been represented by 48-second samples, simulating the HEOS data to enable a valid comparison between the two separate and dissimilar sampling systems. Attention is directed to the appearance of several segments of time, e.g., 0400-0410, during which $B_{OGO} > B_{HEOS}$. Recall that OGO was the more distant from the earth of the two spacecraft, and it follows that the q-parallel magnetic structure is one in which neither field average nor oscillation amplitudes necessarily decrease with distance outward from the earth. In this case, of course, there could have been lateral dependences of B, and we cannot say what profile would have been recorded along a common normal.

The polarizations of q-parallel pulsations perpendicular to $\underline{B}$, the thickness of the oscillation region, and the seemingly irregular independence of B on distance suggest that the q-parallel magnetic structure may be thought

of as a relaxation of the q-perpendicular shock field jump into large amplitude, transverse waves spreading out along $\underline{B}$. A spectrum of frequencies is present which, together with the dispersive quality of local wave propagation, results in a complicated pattern of wave superpositions, sometimes adding to very large field values, sometimes cancelling to nearly zero magnitude. "Shocks", i.e., steep gradients with irreversible plasma changes, may be forming, dispersing, and reforming locally all along a broad front.

Plasma Structure

The distinct character of the q-parallel structure has been elucidated in large part by the behavior of the plasma. Perhaps the most serious deficiency in plasma detection on either spacecraft was the inability to obtain accurate directional spectra. Without these it has not been possible to determine just where the protons transferred from the peak to the wings of the solar wind distribution were heading. Since we know that reflected protons of energy more than double the bulk speed are associated with upstream waves, and very likely with the effective viscosity responsible for dissipation in supercritical shocks, it is attractive to infer that the high energy tail of the proton spectra represented particles reflected in one or more magnetic gradients and travelling in directions other than that of the local bulk flow. In a strict sense, however, we have obtained only a one-dimensional view of the plasma, and what we have seen is the "energy" or "speed structure" of the q-parallel shock: The solar wind is slowed down at most only a little, while a significant fraction of the streaming protons are scattered to both higher and lower speeds, in the spacecraft frame. Some of these contribute to a substantial high-energy tail. In addition, we know that the bulk flow is deflected appreciably, often 20° to 40° or more, by encounters with large amplitude field pulsations.

There were no electron data accessible to this study, the London Langmuir probe record being especially difficult to interpret at the 1 kilobit telemetry rate. However, we note that the data from the outbound, apparently quasi-parallel, shock passage by Mariner 10 at Mercury suggest electron density and activity that were different from those associated with either the solar wind or the magnetosheath (Bridge, et al., 1974). Such a separate identity would be consistent with the observations by other diagnostics in the present study.

Wave Structure

Electric and magnetic waves appear to have been distingusihed in our q-parallel structure by the absence of any outstanding intrinsic values. We note especially that only once did plasma wave noise exceed briefly, 10 mV/m, and rarely did it exceed 2-3 mV/m. This may be contrasted with the almost steady noise at 5-10 mV/m recorded in very high-β shocks (Formisano et al., 1975), and with the very high electric fields in high mach number, q-perpendicular shocks (Greenstadt, 1974). Similarly, the magnetic ELF noise was at lower values than those usually found at elevated β (Greenstadt, 1974). In general, the wave components of the structure were comparable to those associated with simple, laminar, q-perpendicular shocks (Greenstadt et al., 1975). The most interesting wave "structure" was the presence of noise above solar wind background in the interpulsation segments of the data, but the levels of the noise were not striking.

Theoretical Considerations

A comprehensive comparison of observational details with the theory of the microstructure of the quasi-parallel shock is outside the scope of

and that influential upstream non-parallel effects, which some theories have neglected, must be taken into account in seeking a valid theoretical understanding of the parallel bow shock.

Second, $\overline{B}$, as adopted, was within a few degrees of the nominal normal, probably as close to parallel as experimental techniques can certify, but $\theta_{nB} \neq 0$, and the question can be raised that the observed shock was not strictly parallel, a geometric condition which may have unique, narrowly defined characteristics. However, the bow shock is a three-dimensional curved "surface" and can never be tightly parallel except over a minor fraction of its area. Since theoretical and numerical results have been one-dimensional, it is unknown, given deflected flux, propagating waves, and reflected particles, to what extent the untidy nearly-parallel structure we observed would spread into and destroy any adjacent "clean" parallel structure if it existed. We favor the notion that dimensional effects are important in the bow shock and that locally parallel, unlike perpendicular, average geometry may not be an isolatable state.

Finally, there were some resemblances and dissimilarities of the observations to existing theory that must be noted. The high β, low M calculations of Auer & Völk (1973) developed a genuine shock with a density jump, but the jump was accompanied by an increase in the pressure anisotropy. The enhanced anisotropy would support the firehose instability which would in turn provide a dissipation mechanism and form the parallel shock into a "relaxation" phenomenon with appreciable magnetic turbulence. The authors proposed a qualitative extrapolation to strong (high M) parallel shocks in which they envisioned a double structure consisting of a thin electrostatic

shock ($\Delta X \approx \lambda_D$), distinguished by a density and temperature jump, followed downstream by a broad relaxation structure of the firehose type ($\Delta X \approx 100\ R_i$). They speculated that the magnetosheath itself could be the relaxation zone of the bow shock. In support of this argument, we recall the HEOS plasma measurements of Fig. 3, where the density (and "temperature" as well) was commonly higher throughout the pulsation interval than it was in what we adopted as the undisturbed solar wind. This result is consistent with the idea that magnetic turbulence would exist behind an electrostatic shock and within a region of enhanced density. If the density enhancements in the pulsation structure were shock-connected and not merely interplanetary effects accompanying other, unidentified discontinuities in the observation interval, then the important electrostatic part of the Auer & Völk model might have been responsible.

Are there any measured or inferred quantities of the 14th that can be brought to bear on the Kennel-Sagdeev/Auer-Völk theories? As already noted, none of the most salient quantities was directly measured, let alone measured independently upstream, but we can estimate some rough limits. The condition on firehose instability, assuming isotropic T_e, is that $\Delta = (T_{i\|} - T_{i\perp}) - 2/\beta_i > 0$. Even if $T_\perp/T_\| = 0$, it would be necessary that $\beta_i > 2$ to satisfy this condition. Outside the pulsations at HEOS, the highest β_i estimated was on the order of 0.6, so, even if $T_{i\perp}/T_{i\|} = 0$, $\Delta \lesssim -2.33$, which would not have provided even marginal instability before solar wind encounter with some shock feature. Within the pulsation structure at HEOS, computer estimates from the irregular spectral distributions gave three cases (out of 17) in which $\beta_i > 2$. If the temperatures associated with these cases were

assigned to $T_{||}$, i.e., if all the apparent local proton heating had contributed to $T_{||}$ only, and if we take as $T_{\perp}$ the value 6.4×10^4°K, which was the lowest temperature estimated for any case during the interval, the three cases give $\Delta = .4, .4$, and $.05$. Thus, the possibility exists that ion heating within the q-parallel structure might have created some locally firehose-unstable conditions, given some extreme assumptions about the nature of the heating and the values of local parameters. This is hardly the kind of evidence with which we can say the model of Auer & Völk was supported by the data. We must add to this the observational fact that even though outer pulsations next to upstream waves were recorded at OGO, no extraordinary plasma wave (acoustic) noise was encountered and no extreme proton heating was seen there. Moreover, at high resolution, thermalized protons and high B tended to occur together, cancelling each other out in the definition of β_i, so that β_i did not appear likely to reach high values unless created by computer in the averaging process. The condition $\Delta > 0$ was therefore improbable on qualitative empirical grounds.

On balance, we cannot rule out the possibility that the firehose instability may have been excited locally at some times, but we do not believe the electrostatic/firehose relaxation shock model was applicable to the case described in this report in the sense of accounting for the observed overall macrostructure. We suggest that most, if not all, of the quasi-parallel macrostructure we observed was part of a largely upstream, unshocked, or partially shocked plasma state in which the shock relaxed to a thick region with waves, and probably reflected particles, extending far into the upstream medium, and with large amplitude transverse pulses and waves deflecting and

partially thermalizing, through ion waves in their gradients, the incoming solar wind. We propose that separated pulses formed and steepened and that the solar wind streamed through these, emerging as a modified plasma flow corresponding to the interpulsation regime described in the report. The only dissipation mechanisms for which direct evidence was recorded in the region observed were dispersion and ion plasma frequency noise. We speculate that the highest estimated proton temperatures could have been produced by multiple pulsation encounters and anomalous ion-wave resistivity only, and that these were the most likely components of the q-parallel microstructure. The shock appeared superficially as one in which whistlers might have taken the otherwise abrupt transition and run away upstream with it, spreading fragments along the way. This interpretation would be in closest accord with the picture of oblique whistler shocks presented by Tidman & Krall (1971). The upstream conditions in our observed case corresponded to region IV, near the b_x axis, of their Figs. 5.3 and 9.4 and the shock profile corresponded to the forward section including part of the dissipative shock layer, in the sketch of their Fig. 9.5. In addition, we would expect a complex interaction among solar wind particles, reflected protons and electrons, upstream Alfvén waves, and whistlers propagating both upstream and downstream. The picture of Biskamp & Welter (1972) comes to mind, but we lack the diagnostic sophistication for testing their model. We do not exclude two-stream interactions.

SUMMARY

The observed quasi-parallel bow shock structure, at supercritical mach number and moderate β, was characterized as follows:

1. Irregular, large amplitude, magnetic pulsations, sometimes in bursts, often separated by intervals of smaller amplitude, upstream-like waves;

2. Thickness $\gtrsim 2\ R_E$;

3. Large amplitude, quasiperiodic, transverse magnetic wave components;

4. Solar wind of nominally unreduced, but significantly deflected, streaming velocity;

5. Solar wind of elevated temperature, enhanced density, distinct distribution with skewed high energy tails and irregular low energy envelopes;

6. Inversely related plasma flux and field magnitudes;

7. Electric and magnetic ELF wave noise comparable to that associated with laminar shocks;

8. Interpulsation regions of upstream magnetic magnitude and wave structure but noisy, deflected, and partially thermalized plasma flow;

9. No direct evidence that the macrostructure was governed by firehose instability as a dissipation mechanism;

10. Macrostructure following the outlines of an oblique whistler shock, modified by additional irregularity and complexity.

ACKNOWLEDGEMENTS

Valuable discussions with R. W. Fredricks and support of NASA Contract NASW-2398 were essential to this study.

REFERENCES

Auer, R. D., and H. J. Völk, Parallel high β shocks and relaxation phenomena, Astrophys. & Space Sci., 22, 243, 1973.

Biskamp, D., and H. Welter, Structure of the earth's bow shock, J. Geophys. Res., 77, 6052, 1972.

Bonetti, A., G. Moreno, S. Cantarano, A. Egidi, R. Marconero, F. Palutan, and G. Pizzella, Solar-wind observations with satellite ESRO-HEOS-1 in December 1968, Nuovo Cimento, Serie X, 64B, 307, 1969.

Crook, G. M., F. L. Scarf, R. W. Fredricks, I. M. Green, and P. Lukas, The OGO 5 plasma wave detector: Instrumentation and in-flight operation, IEEE Trans. Geosci. Electron., GE-7, 120, 1969.

Fairfield, D. H., Average and unusual locations of the earth's magnetopause and bow shock, J. Geophys. Res., 76, 6700, 1971.

Fairfield, D. H., and W. C. Feldman, Standing waves at low mach number laminar bow shocks, J. Geophys. Res., 80, 515, 1975.

Formisano, V., The earth's bow shock fine structure, Correlated Interplanetary and Magnetospheric Observations, VII ESLAB Symposium (Ed. D. E. Page), Reidel, Dordrecht, Holland, 1974.

Formisano, V., G. Moreno, F. Palmiotto, and P. C. Hedgecock, Solar wind interaction with the earth's magnetic field: 1. Magnetosheath, J. Geophys. Res., 78, 3714, 1973.

Formisano, V., and P. C. Hedgecock, Solar wind interaction with the earth's magnetic field, 3. On the earth's bow shock structure, J. Geophys. Res., 78, 3745, 1973a.

Formisano, V., and P. C. Hedgecock, On the structure of the turbulent bow shock, J. Geophys. Res., 78, 6522, 1973b.

Formisano, V., C. T. Russell, J. D. Means, E. W. Greenstadt, F. L. Scarf, and M. Neugebauer, Collisionless shock waves in space: A very high-β structure, J. Geophys. Res., in press, 1975.

Formisano, V., C. T. Russell, J. D. Means, F. L. Scarf, and M. Neugebauer, The perpendicular bow shock, Draft Report, to be submitted, 1975.

Greenstadt, E. W., I. M. Green, G. T. Inouye, D. S. Colburn, J. H. Binsack, and E. F. Lyon, Dual satellite observations of the earth's bow shock, 1. The thick pulsation shock, Cosmic Electrodyn., 1, 160, 1970a.

Greenstadt, E. W., I. M. Green, G. T. Inouye, D. S. Colburn, J. H. Binsack, and E. F. Lyon, Dual satellite observations of the earth's bow shock, 3. Field-determined shock structure, Cosmic Electrodyn., 1, 316, 1970b.

Greenstadt, E. W., Observations of nonuniform structure of the earth's bow shock correlated with interplanetary field orientation, J. Geophys. Res., 77, 1729, 1972a.

Greenstadt, E. W., Binary index for assessing local bow shock obliquity, J. Geophys. Res., 77, 5467, 1972b.

Greenstadt, E. W., Structure of the terrestrial bow shock, Solar Wind Three, Proc. Third Solar Wind Conf., Asilomar (Ed. C. T. Russell), Inst. Geophys. & Planet. Phys., UCLA, 440, 1974

Greenstadt, E. W., C. T. Russell, F. L. Scarf, V. Formisano, and M. Neugebauer, Structure of the quasi-perpendicular, laminar bow shock, J. Geophys. Res., 80, in press, 1975.

Harris, K. K., and G. W. Sharp, OGO 5 ion spectrometer, IEEE Trans. Geosci. Electron., GE-7, 93, 1969.

Hedgecock, P. C., Magnetometer experiments in the european space research organisation's HEOS satellites, Space Sci. Instrumentation, 1, 61, 1975.

Kellogg, P. J., Flow of plasma around the earth, J. Geophys. Res., 67, 3805, 1962.

Kellogg, P. J., Solitary waves in cold, collisionless plasma, Phys. Fluids, 7, 1555, 1964.

Kennel, C. F., and R. Z. Sagdeev, Collisionless shock waves in high β plasmas, 1., J. Geophys. Res., 72, 3303, 1967.

Neugebauer, M., Initial decceleration of solar-wind positive ions in the earth's bow shock, J. Geophys. Res., 75, 717, 1970.

Ogilvie, K. W., J. D. Scudder, R. E. Hartle, G. L. Siscoe, H. S. Bridge, A. J. Lazarus, J. R. Asbridge, S. J. Bame, and C. M. Yeates, Observations of Mercury encounter by the plasma science experiment on Mariner 10, Science, 185, 145, 1974.

Robson, A. E., Experiments on oblique shock waves, Spec. Publ. 51, ESRO, Frascati, Italy, 159, 1969.

Snare, R. C., and C. R. Benjamin, Magnetic field instrument for the OGO-E spacecraft, IEEE Trans. Nucl. Sci., NS-13(6), 1966.

Sonett, C. P., D. L. Judge, and J. M. Kelso, Evidence concerning instabilities of the distant geomagnetic field: Pioneer I, J. Geophys. Res., 64, 941, 1959.

Tidman, D. A., and N. A. Krall, Shock Waves in Collisionless Plasmas, John Wiley-Interscience, New York, 1971.

FIGURE CAPTIONS

Figure 1. Synoptic magnetic field observations of the quasi-parallel bow shock of 14 February 1969. Explorer 35: 82-sec averages; OGO 5: 60-sec averages; HEOS 1: 48-sec samples. Pulsation index I_p was computed with p = 1.6 (Greenstadt, 1972b).

Figure 2. Relative locations of satellite observations and nominal shock curves from various points of view. All distance scales are in units of earth radii (R_E) in solar ecliptic coordinates. The direction of motion along the trajectory segments marked HEOS 1 and OGO 5 was outward for both spacecraft.

Figure 3. Synoptic plasma and field magnitude data from HEOS 1. Each plasma parameter value corresponds to one complete 384-sec spectrum; the circles represent concurrent values from OGO 5.

Figure 4. (a) Average solar wind, magnetosheath, and pulsation region ion energy spectra from HEOS 1; (b) Comparison of pulsation ion spectra with composite envelope of solar wind and sheath spectra; (c) Two representative pulsation ion spectra.

Figure 5. (a) Comparison of solar wind flux with field magnitude at OGO 5; (b) Apparent inverse relationship between flux and field strength in quasi-parallel structure from 0355 to 0515.

Figure 6. Individual ion spectra (solid lines) from HEOS 1 in original time sequence, displaying the four spectral subcycles in each. The top panel identifies the times and conditions at which the spectra were obtained relative to the q-parallel structural sequence recorded by the HEOS

magnetometer. Dashed and dotted lines reproduce the average solar wind and magnetosheath spectra at lower right.

Figure 7. Magnetosheath (left) and pulsation samples of field components measured by OGO 5 (UCLA), showing persistence of preferred wave polarizations normal to $\underset{\sim}{B}$. $\overline{\underset{\sim}{B}}$ is along B_X at left, along B_Z at right.

Figure 8. Multidiagnostic views of various shock conditions seen by OGO 5 on 14 February 69.

(a) quasi-perpendicular crossing

(b) quasi-parallel field gradient

(c) two samples (left and right) of upstream wave region and two samples (center) of "interpulsation" wave regions

(d) two samples of pulsation bursts

(e) two samples of segments of long pulsation trains.

Figure 9. Simultaneous 48-sec samples of quasi-parallel structure seen by HEOS and OGO magnetometers, showing alternation of higher field level at the two spacecraft.

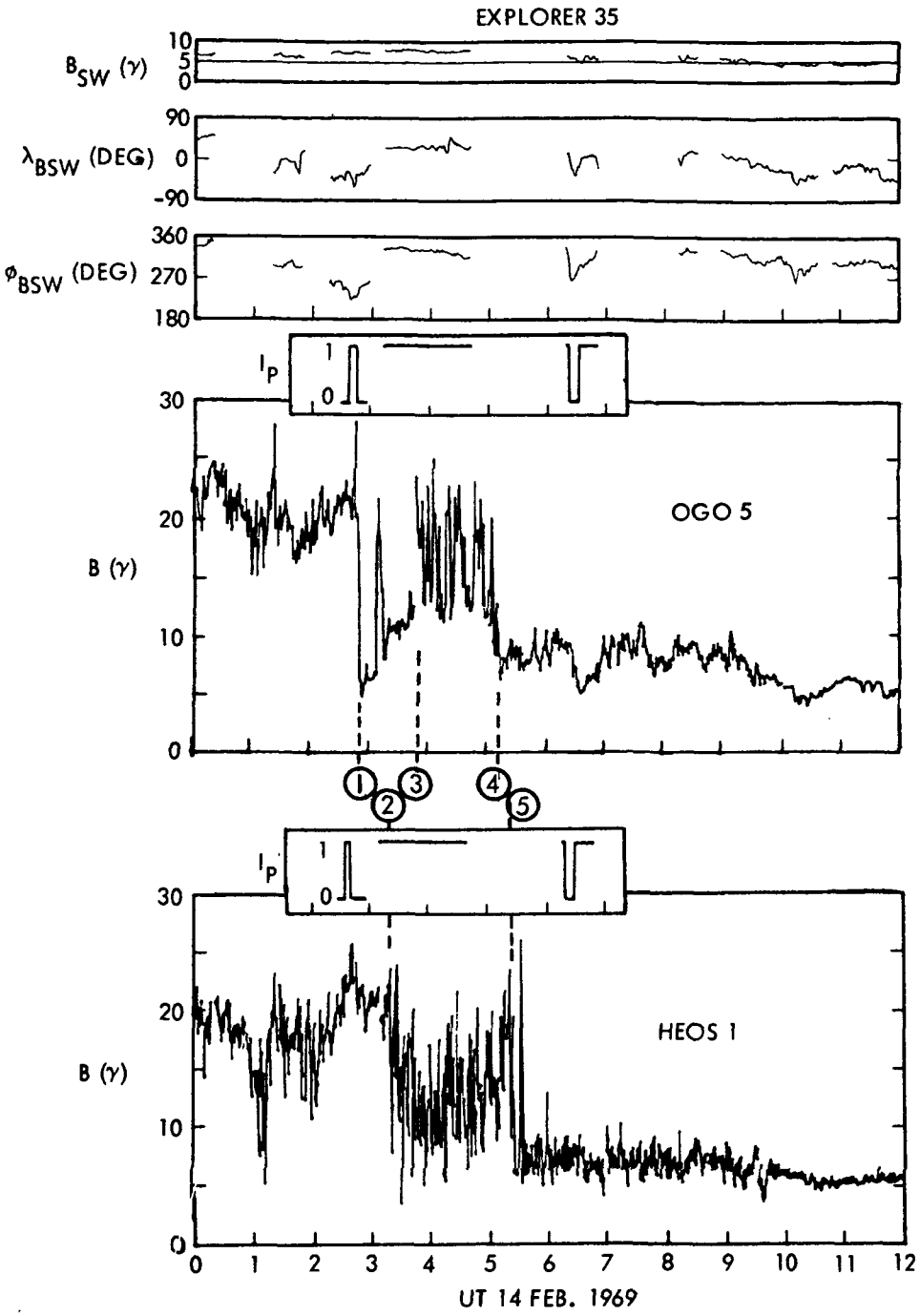

Figure 1. Synoptic magnetic field observations of the quasi-parallel bow shock of 14 February 1969. Explorer 35: 82-sec averages; OGO 5: 60-sec averages; HEOS 1: 48-sec samples. Pulsation index I_p was computed with $p = 1.6$ (Greenstadt, 1972b).

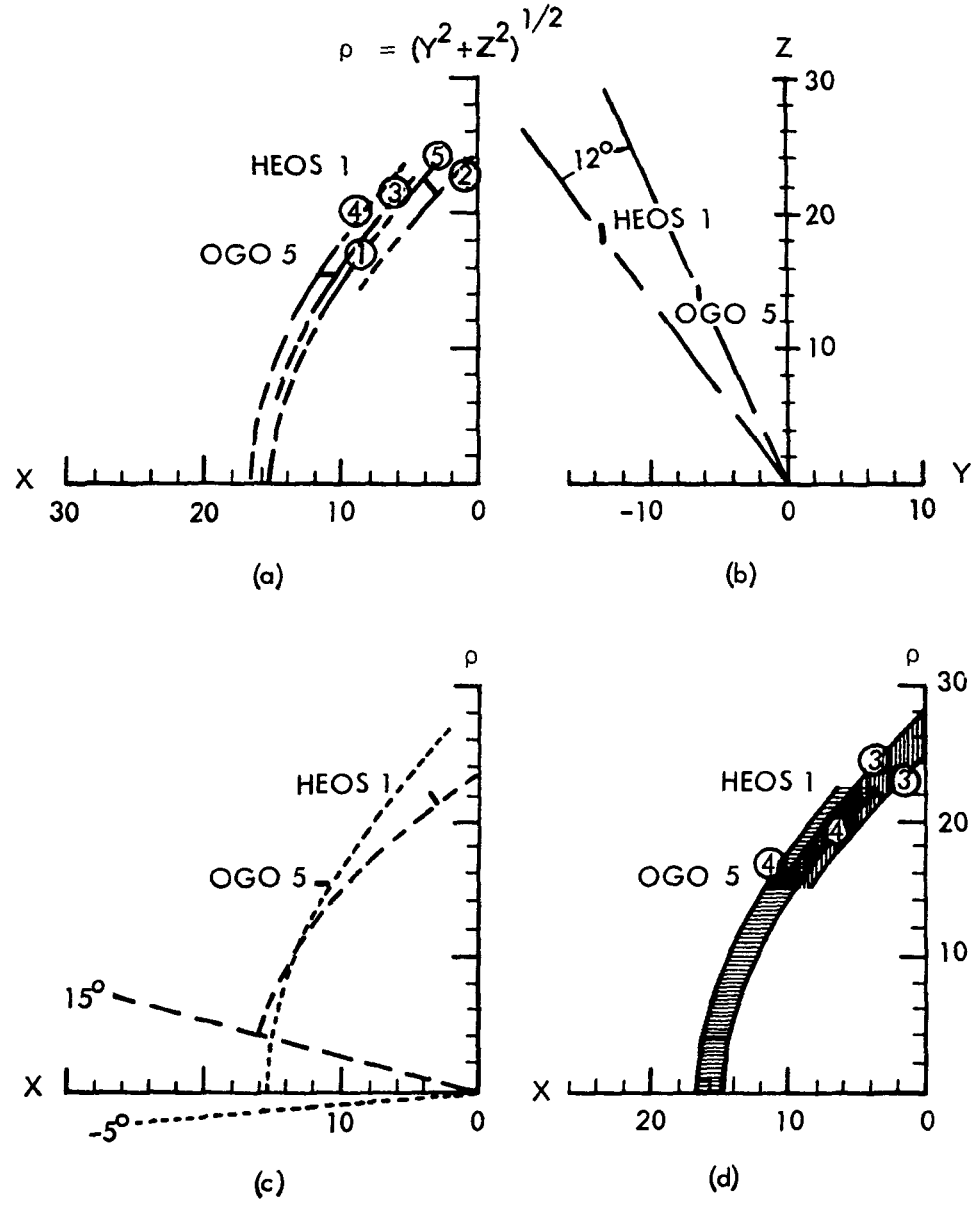

Figure 2. Relative locations of satellite observations and nominal shock curves from various points of view. All distance scales are in units of earth radii (R_E) in solar ecliptic coordinates. The direction of motion along the trajectory segments marked HEOS 1 and OGO 5 was outward for both spacecraft.

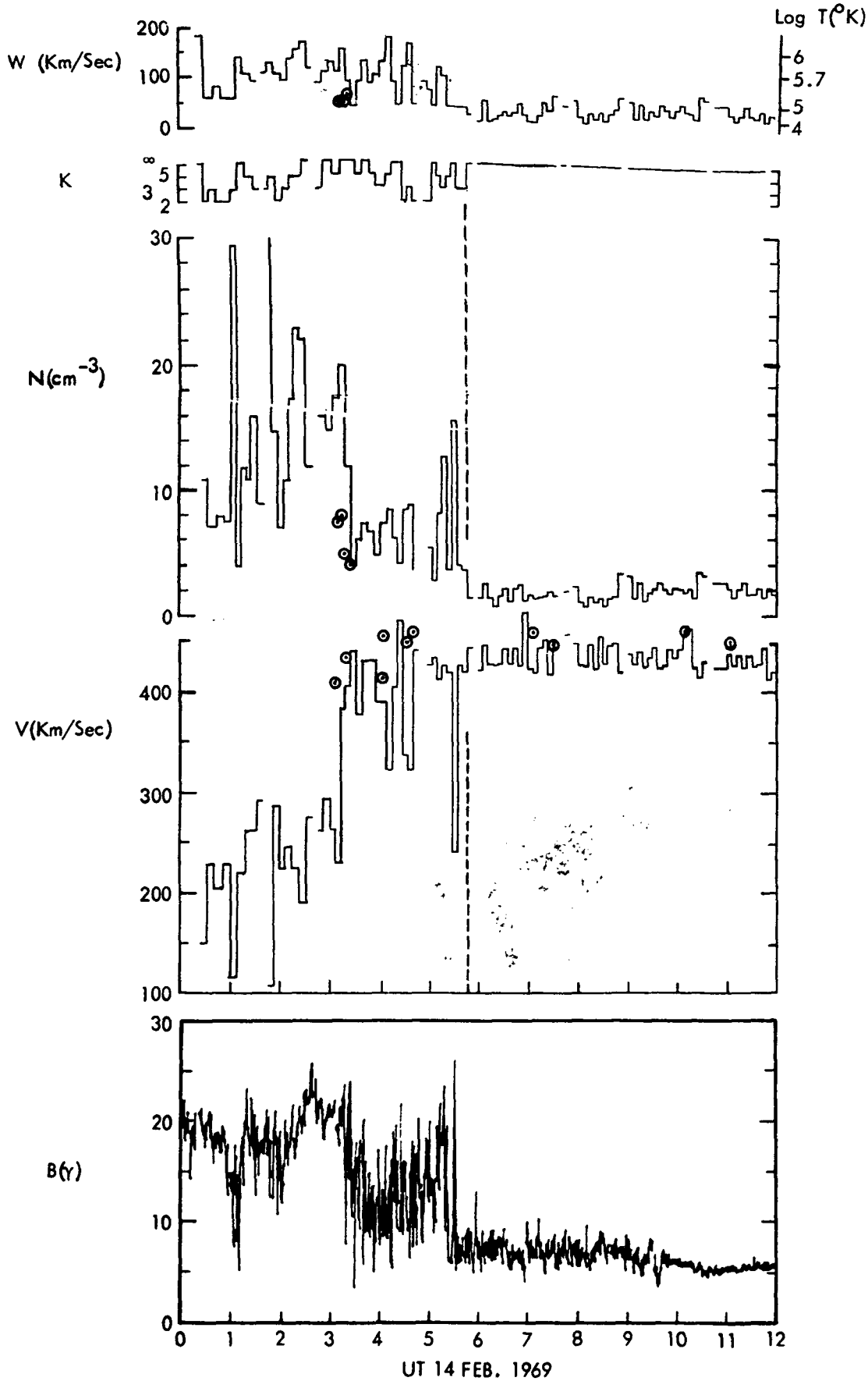

Figure 3. Synoptic plasma and field magnitude data from HEOS 1. Each Plasma parameter value corresponds to one complete 384-sec spectrum; the circles represent concurrent values from OGO 5.

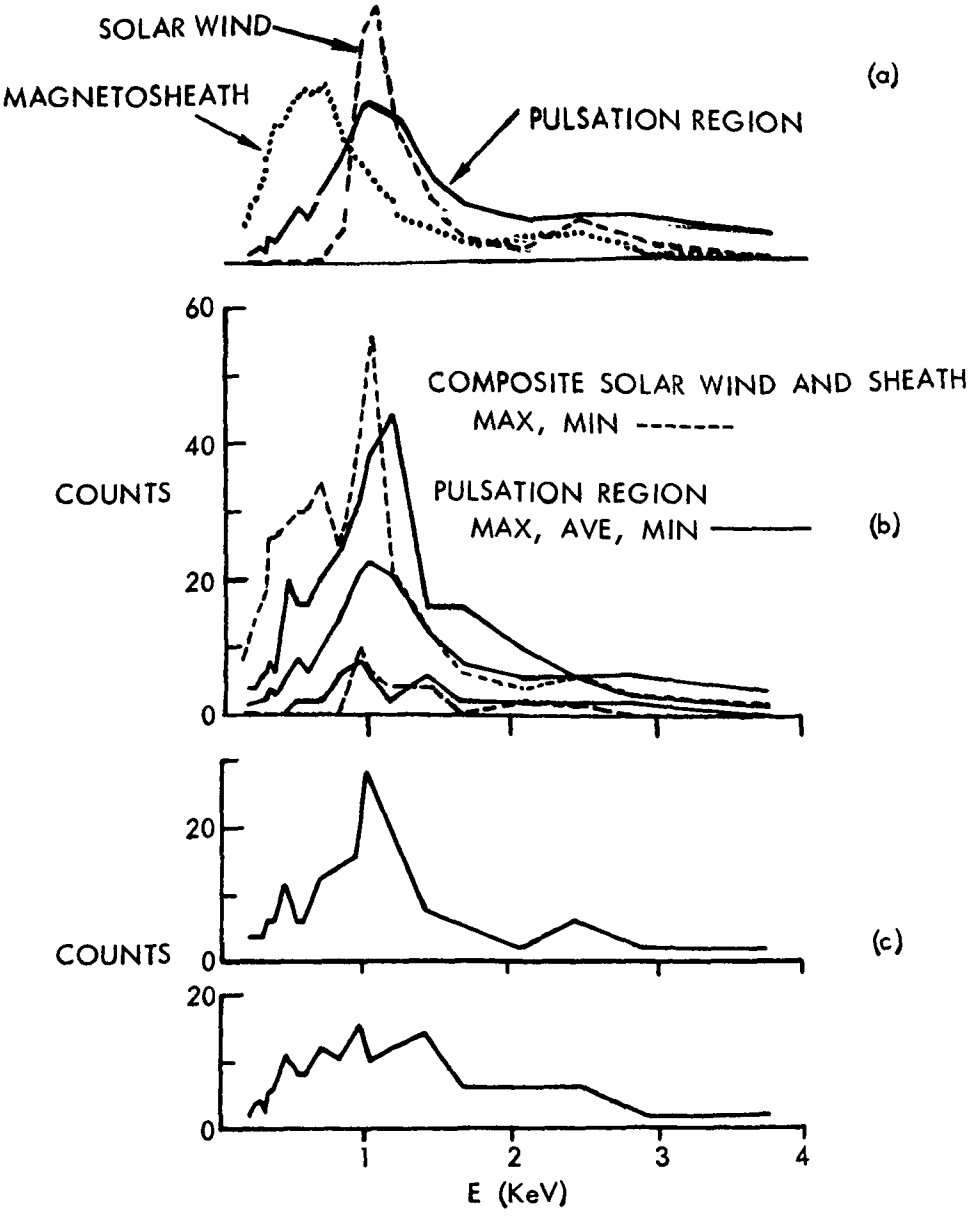

Figure 4. (a) Average solar wind, magnetosheath, and pulsation region ion energy spectra from HEOS 1; (b) Comparison of pulsation ion spectra with composite envelope of solar wind and sheath spectra; (c) Two representative pulsation ion spectra.

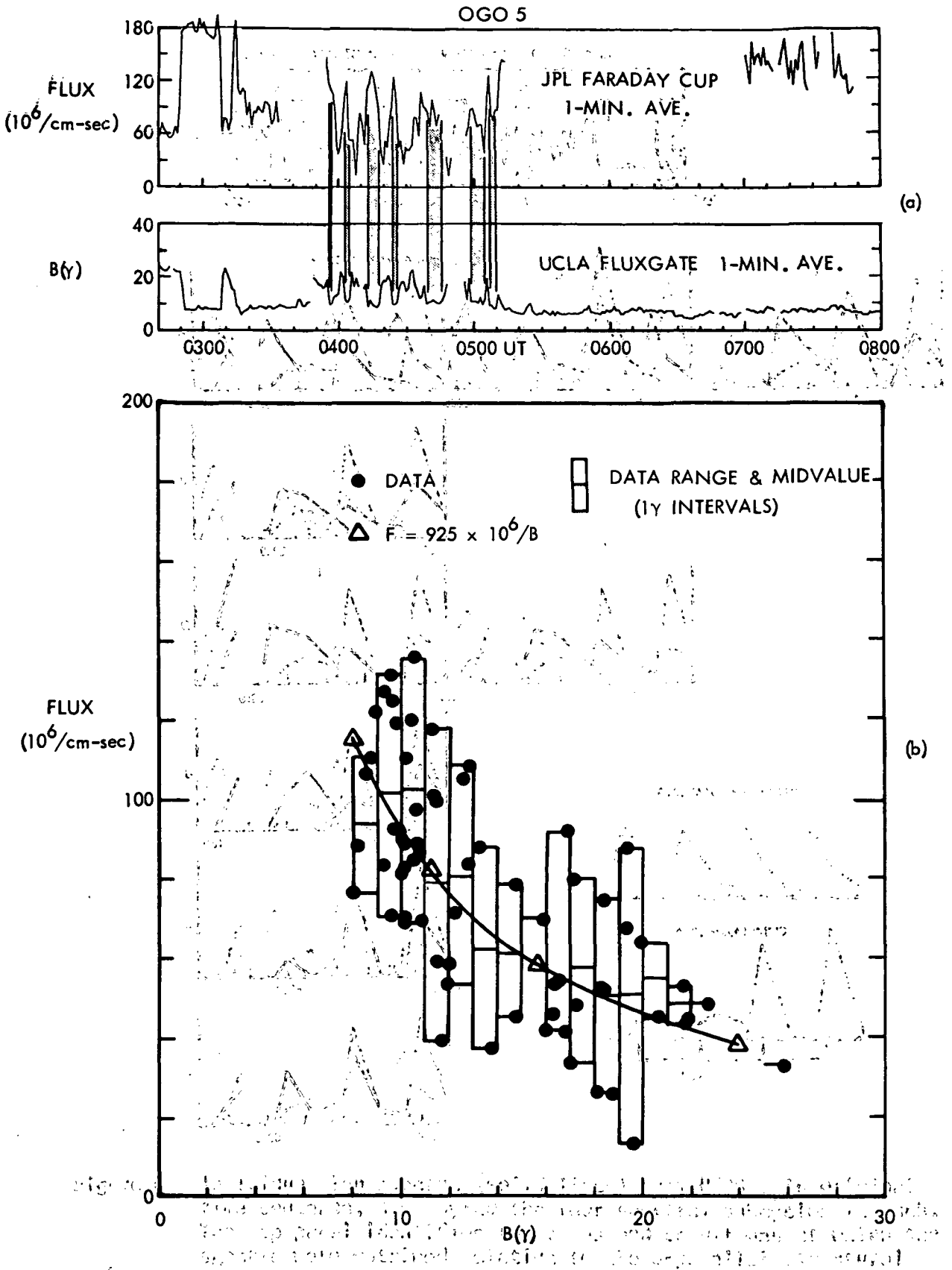

Figure 5. (a) Comparison of solar wind flux with field magnitude at OGO 5; (b) Apparent inverse relationship between flux and field strength in quasi-parallel structure from 0355 to 0515.

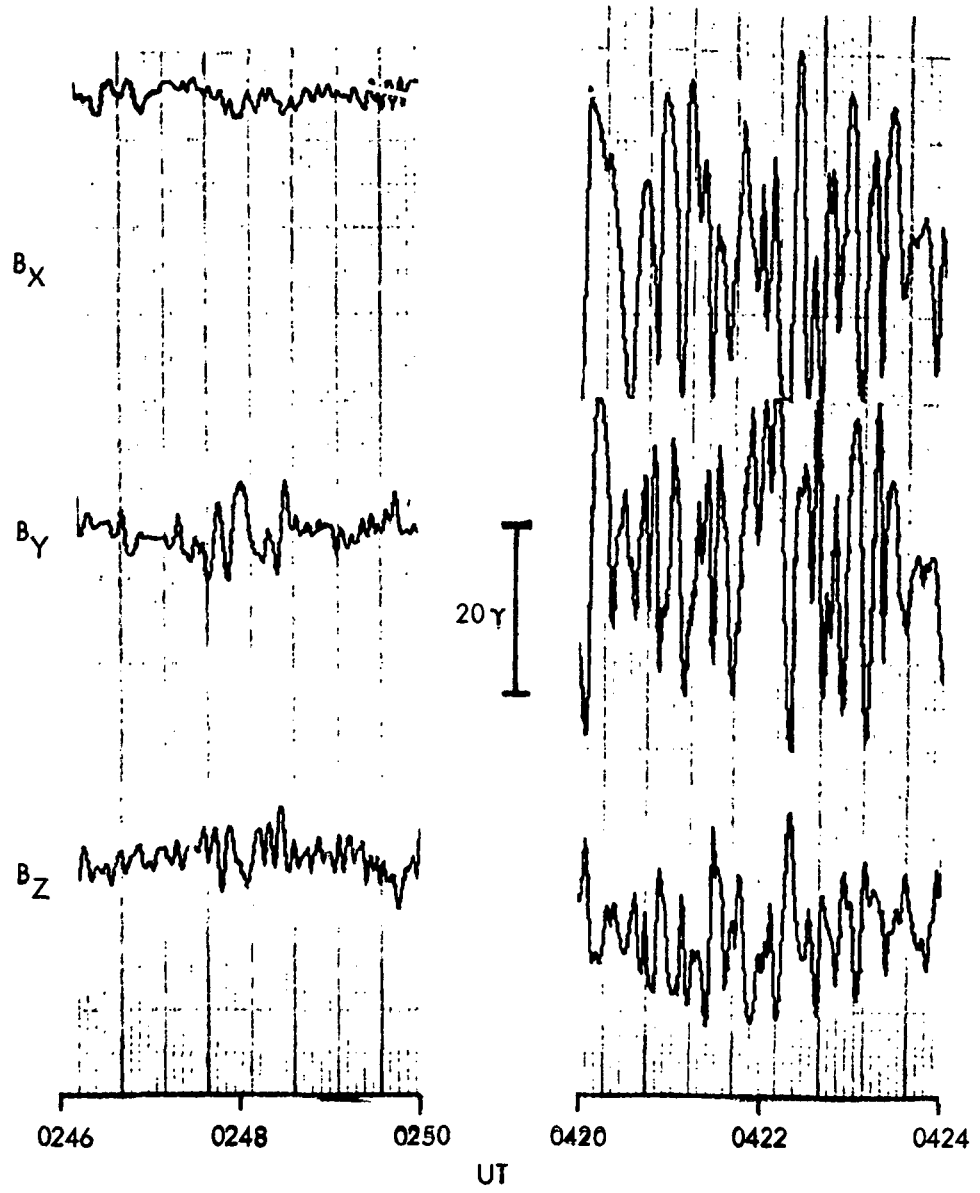

Figure 7. Magnetosheath (left) and pulsation samples of field components measured by OGO 5 (UCLA), showing persistence of preferred wave polarizations normal to $\underset{\sim}{B}$. $\underset{\sim}{B}$ is along B_X at left, along B_Z at right.

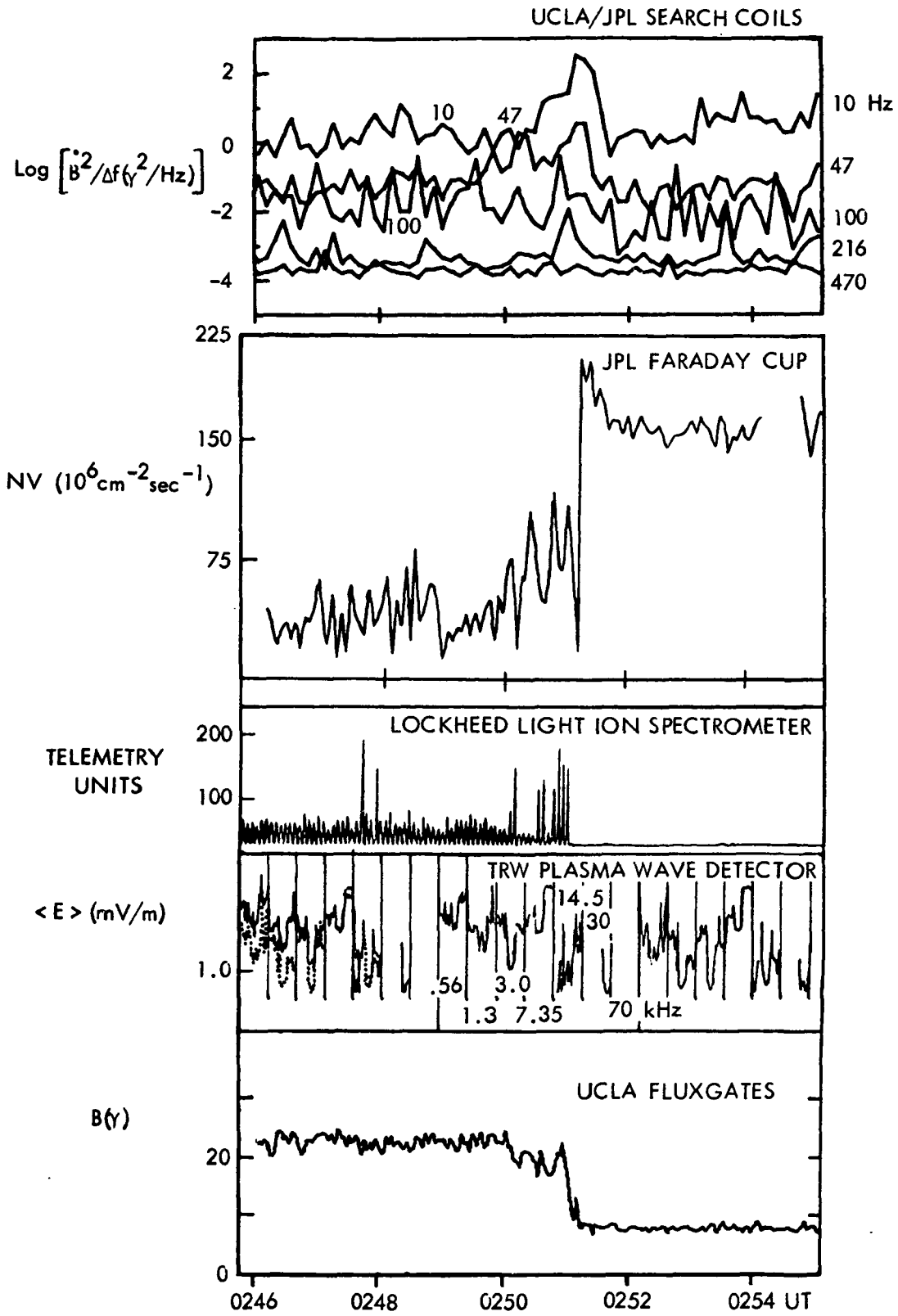

Figure 8. Multidiagnostic views of various shock conditions seen by OGO 5 on 14 February 69.

(a) quasi-perpendicular crossing

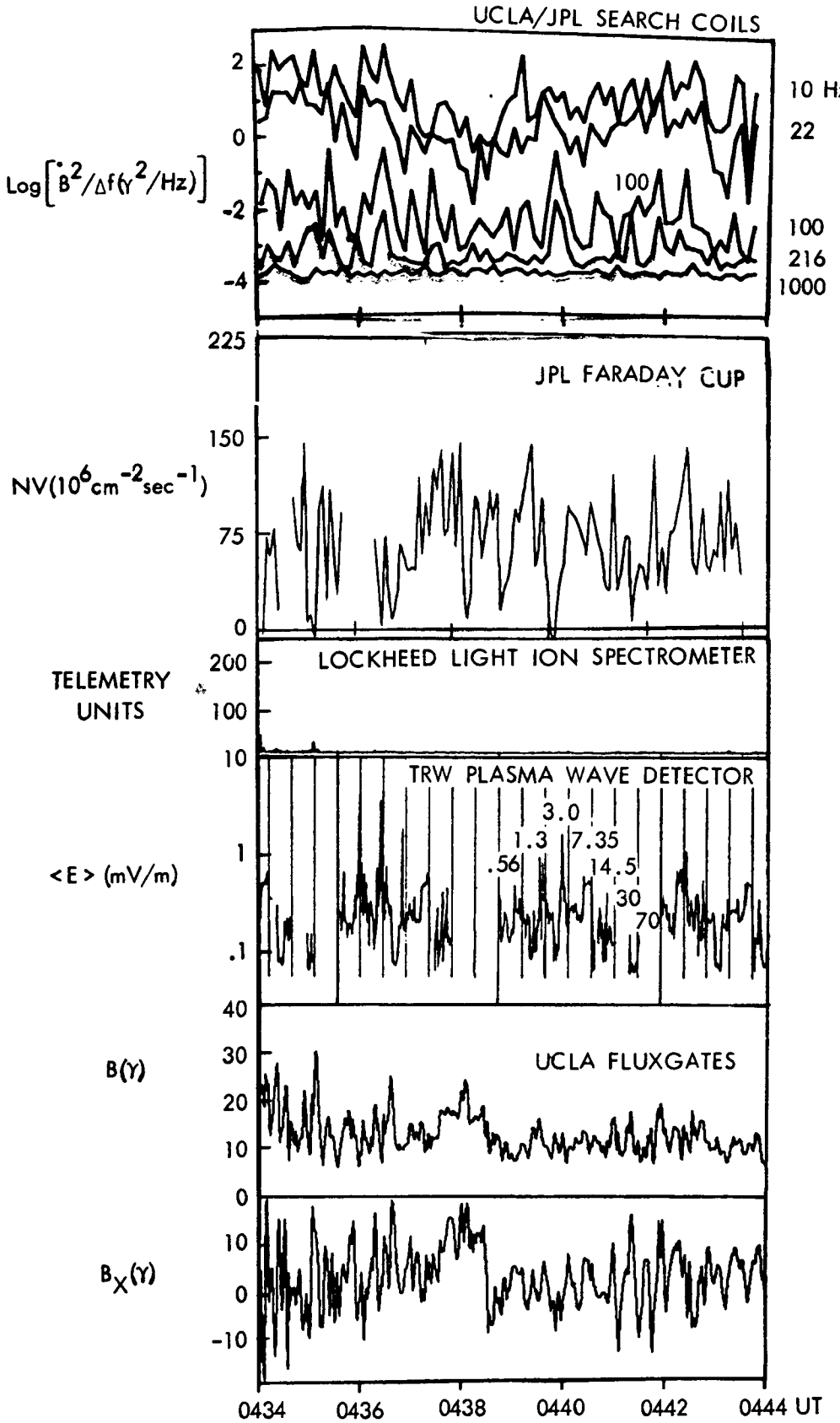

Figure 8(b) quasi-parallel field gradient

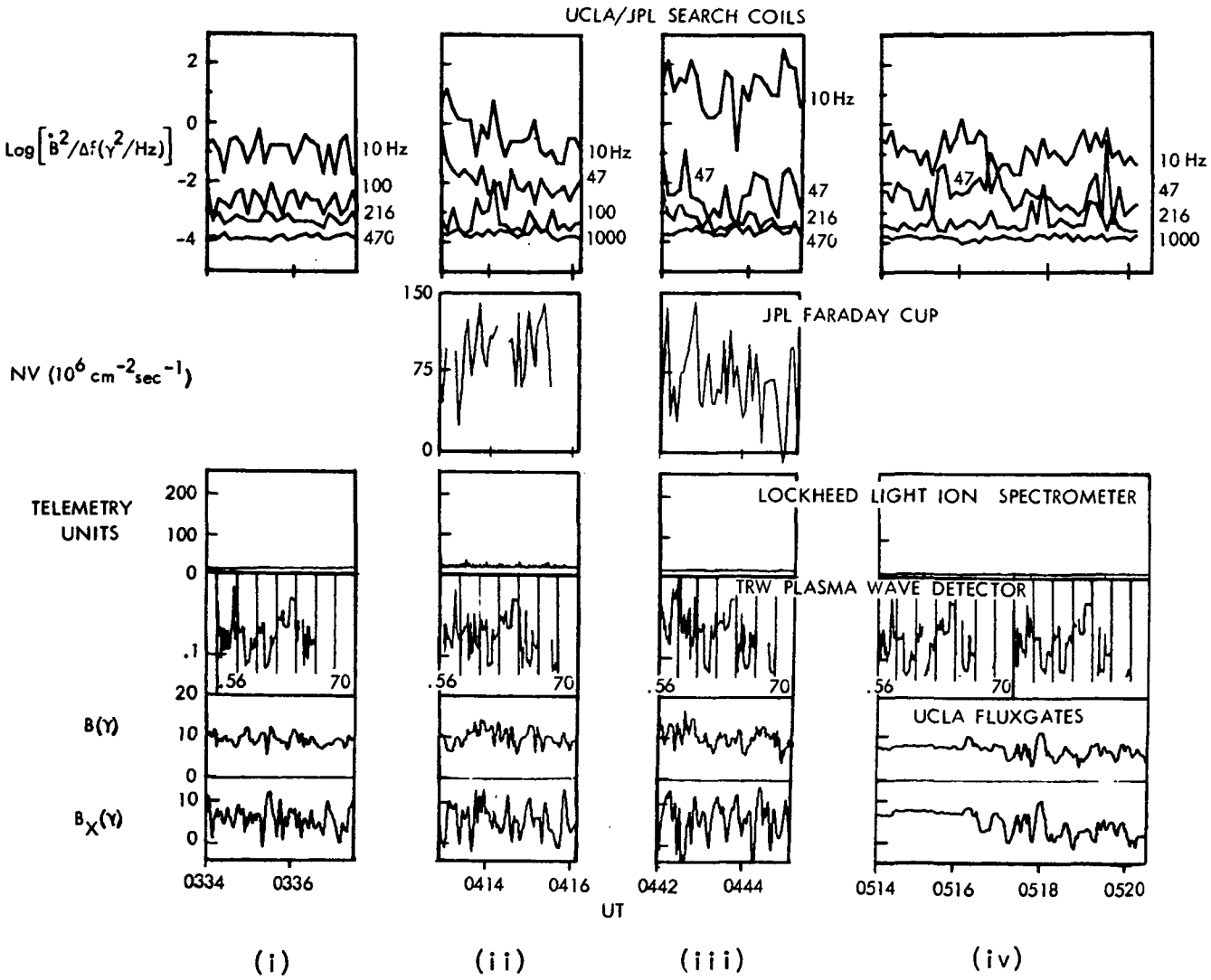

Figure 8(c) two samples (left and right) of upstream wave region and two samples (center) of "interpulsation" wave regions

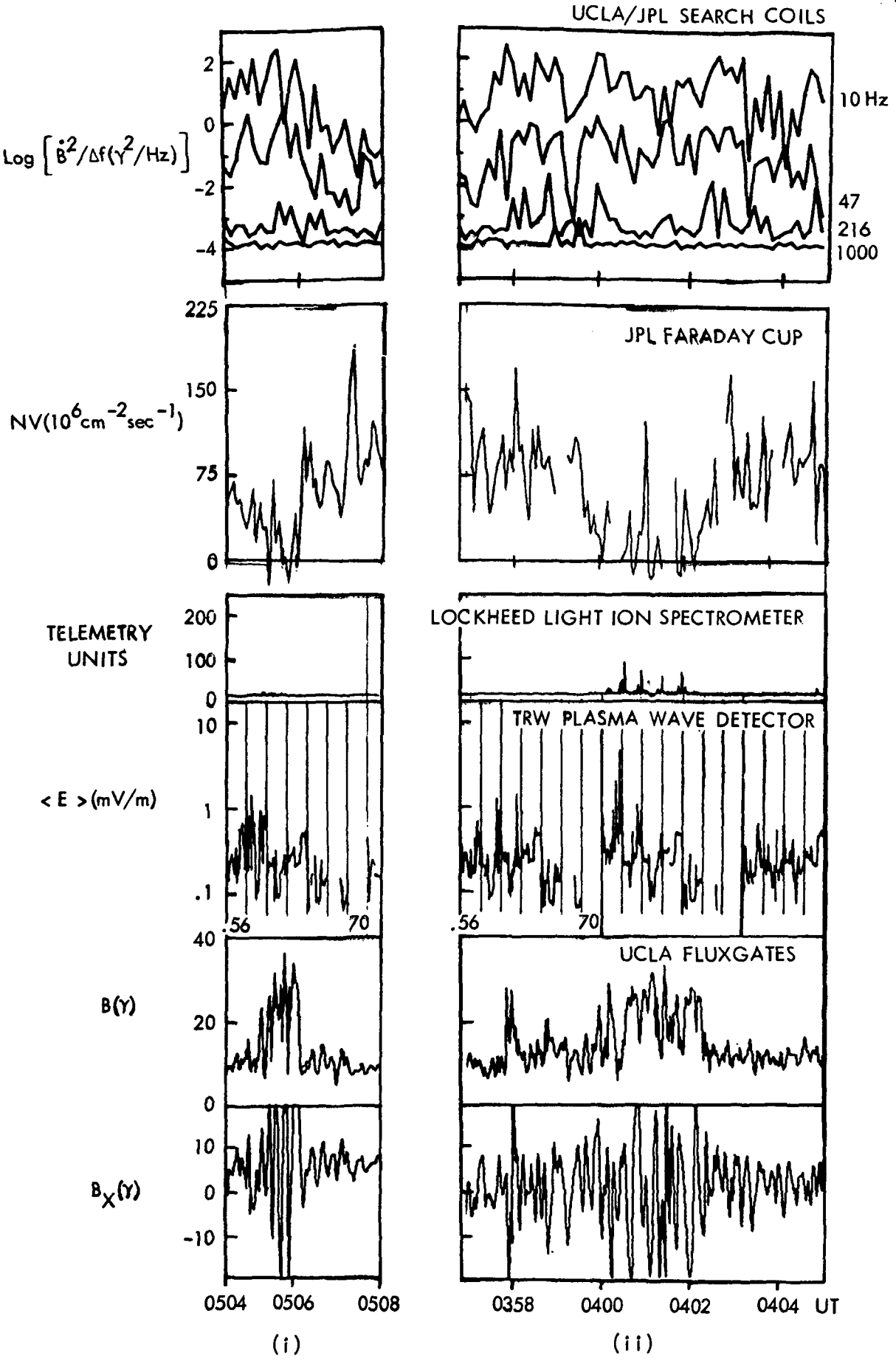

Figure 8(d) two samples of pulsation bursts

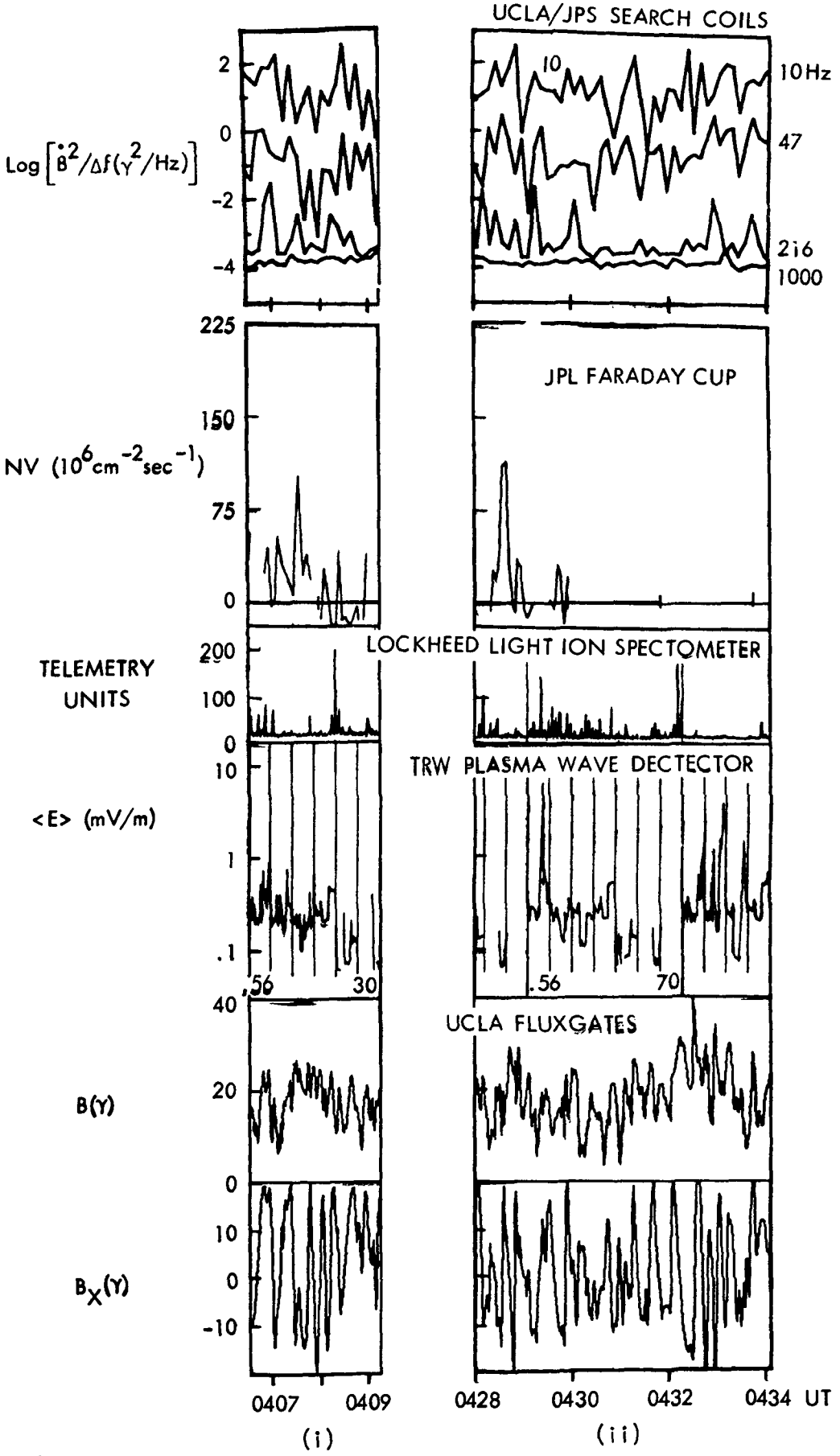

Figure 8(e) two samples of long pulsation trains

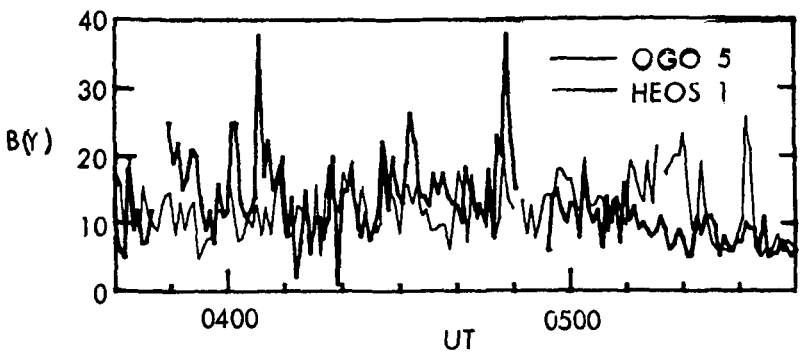

Figure 9. Simultaneous 48-sec samples of quasi-parallel structure seen by HEOS and OGO magnetometers, showing alternation of higher field level at the two spacecraft.

APPENDIX C

THICKNESS OF MAGNETIC STRUCTURES ASSOCIATED WITH THE EARTH'S BOW SHOCK

D. L. Morse

Laboratory of Plasma Studies, Cornell University,
Ithaca, New York 14850

E. W. Greenstadt

Space Sciences Department, TRW Systems
Redondo Beach, California 90278

ABSTRACT

The thickness of magnetic structures associated with quasi-perpendicular bow shocks has been observed to vary over more than two orders of magnitude. In this paper we employ an instability criterion which states that the magnetic structure of perpendicular shocks adjusts itself to keep electrostatic waves excited by the relative drift of electrons and ions at marginal stability. The marginal stability boundary and measured plasma parameters are used to calculate the expected thickness of bow shock magnetic structures. The calculated and measured thickness are compared and found to be in good agreement over a range from less than 10 km to greater than 500 km. The conclusion is that the thickness of magnetic structures associated with quasi-perpendicular bow shocks is determined primarily by dissipation due to electron-ion streaming instabilities, rather than by dispersive effects.

INTRODUCTION

When the angle θ_{nB} between the solar wind magnetic field and the local bow shock normal exceeds 50° or so, the magnetic transition is observed in many cases to be "clean" or "abrupt" (Greenstadt, 1974; Fairfield, 1974). Observations have indicated that in such clearly identifiable quasi-perpendicular magnetic shock profiles electrons are heated early in the magnetic gradient and essentially independently of the protons (Montgomery et al., 1970; Neugebauer et al., 1971; Greenstadt et al., 1975). It should be possible therefore to treat at least part of the shock structure in terms of electrostatic waves thought responsible for electron heating alone. In this note we choose a simple wave model and compare computed and measured thicknesses of the magnetic gradient for some laminar (low M, low β) cases in which ion heating is minimal anyway (Formisano et al., 1973) and for one case which tests the applicability of the model to a high M, high β magnetic gradient. The cases selected provided shock thicknesses estimated independently from experimental data.

ANALYSIS

The diagram of Figure 1 shows an idealized view of the variation of the transverse component of magnetic field through the shock and defines the conventional measure of shock thickness, L_s. Using the differential form of Ampere's law, $\nabla \times \underset{\sim}{B} = \mu_o \underset{\sim}{j}$, we connect the field gradient to the current, and thus to the relative drift velocity V_d:

$$\frac{\partial B_z}{\partial X} = \mu_o j_y, \quad \text{i.e.,} \quad \frac{\Delta B_z}{\Delta X} = \mu_o n e v_d.$$

Thus shock thickness L_s is converted to a gradient scale length,

$$L_s = \Delta X = \frac{\Delta B_z}{\mu_o n e v_d} .$$

We employ a criterion used by Manheimer and Boris (1972) in relation to laboratory shocks, which states that the drift velocity V_d stays close to the drift velocity V_d^* for marginal stability of electrostatic waves driven by the current. This leads to the expression

$$L_s = \frac{\Delta B}{\mu_o n e v_e f(T_e/T_i)}$$

where $f(T_e/T_i) = V_d^*/V_e$. We have multiplied and divided by the electron thermal velocity v_e in order to bring in $v_d^*/v_e = f(T_e/T_i)$, the marginal stability boundary computed by Fried and Gould (1961).

Figure 2 shows the marginal stability boundary $f(T_e/T_i)$ we use in the denominator of the expression for L_s. For low T_e/T_i the instability is generally known as the two-stream or Buneman mode, and for $T_e/T_i > 10$ it is known as the ion acoustic wave instability. The numbered arrows at the bottom mark the values of T_e/T_i estimated for the five cases selected for this report (cited below).

Since the density n, the electron thermal velocity v_e, and T_e/T_i change through the shock, a range of scale lengths L_s is predicted here for each set of upstream conditions. To calculate this range, we proceed as follows. The first estimate of L_s is derived from the upstream values of n,

v_e, and T_e/T_i. As we progress through the shock n, v_e, and T_e/T_i will increase in a way consistent with the shock conservation relations. The variation of $f(T_e/T_i)$ dominates the behavior of L_s until $T_e/T_i \geq 20$, and L_s increases. For $T_e/T_i > 20$, the product $v_e f(T_e/T_i)$ is constant, and L_s decreases as n increases to its final value. The upper limit of the range of L_s calculated in this way generally exceeds the lower limit by about a factor of 2, not much worse than the uncertainty in the observations. Table 1 displays the elements contributing to the calculation. Cases 1-4 here are cases 1-4 of Greenstadt et al. (1975) for low Mach number, laminar shocks. They are generally thick (100-700 km) because of low density in the solar wind ($n \sim 2$ cm^{-3}) and high T_e/T_i (5 to 10), and their magnetic profiles are amazingly close to the oversimplified sketch of Figure 1. Case 5 uses solar wind parameters typical of the data of Fredricks et al. (1970) in their study of electrostatic turbulence at the bow shock. Here the upstream density is high ($n \sim 10$ cm^{-3}) and T_e/T_i low (1.5). The thickness was estimated to be 5-10 km on the basis of multiple crossings by a single satellite, and fits the calculated range of L_s well. Figure 3 illustrates graphically the results of our calculations. Points are labeled by case number.

In between the extremes of solar wind conditions of our cases we would calculate thicknesses in the 10-100 km range, where many estimates have placed the shock thickness. Such estimates would appear to be valid, although they are usually accompanied by insufficient plasma data to allow a well-defined calculation of L_s.

DISCUSSION

An important assumption in the above is that T_i remains at its upstream value throughout the magnetic transition. Resistive heating in the magnetic gradient of the shock generally heats the electrons preferentially. When strong ion heating is observed, it generally takes place behind the abrupt magnetic structure (Montgomery et al., 1970). The ions will suffer adiabatic heating in the density compression, but this one-dimensional compression will spread the velocity distribution in the direction of the shock normal, and leave the waves (which propagate in the plane of the shock) undisturbed.

A further assumption is that the zero magnetic field stability boundary may be used to predict the excitation of instabilities in magnetized plasma. Manheimer and Boris (1972) justify this assumption on the grounds that the turbulent electric fields associated with the fully-developed instability effectively decouple the electrons from the magnetic field. For bow shock parameters, we note that the frequency of the instability (approximately the ion plasma frequency) exceeds the electron gyro-frequency, and the wavelength of the instability (a few Debye lengths) is smaller than the electron gyro-radius. The assumption therefore seems justified, even for waves in the linear regime.

Still another assumption here is that dispersive effects can be neglected. It must be noted that the emphasis by Greenstadt et al. (1975) and Fredricks et al. (1970) was on shock thicknesses in terms of c/ω_{pe} and c/ω_{pi}, and we recognize that our selected cases include values of θ_{nB} as low as 65°, so that dispersion may have played some role. However, the results

imply that where waves are not clearly dominant, the principal magnetic gradients of quasi-perpendicular shocks are primarily dissipative and their thicknesses may not be directly related to dispersive lengths c/ω_{pe}, c/ω_{pi}.

The remarkable adherence of the points in Figure 3 to the line denoting equality between calculated and observed shock thicknesses suggests to the unwary that the aggregate of assumptions underlying the calculation must be valid. We are not quite prepared to abandon the possibility that violations of the various assumptions may simply have canceled each other out, and we strongly favor the extension of these calculations to other cases whenever the observational data are sufficiently complete to support them. The following conclusions seem reasonably secure, however, on the basis of the present analysis alone, and we note that the first two are consistent with experimental data already obtained independently.

CONCLUSIONS

1. T_i is approximately constant in the magnetic field gradient.
2. Ion heating, if present, occurs behind the magnetic structure.
3. The magnetic thickness (of the principal magnetic gradient) is determined primarily by the stability boundary for current-driven electrostatic waves.

ACKNOWLEDGMENTS

Support was provided by (DLM) and NASA Contract NASW-2398 (EWG).

REFERENCES

Fairfield, D. H., Whistler waves observed upstream from collisionless shocks, J. Geophys. Res., 79, 1368, 1974.

Formisano, V., P. C. Hedgecock, G. Moreno, F. Palmiotto, and J. Chao, Solar wind interaction with the earth's magnetic field. 2. The magneto-hydrodynamic bow shock, J. Geophys. Res., 78, 3731, 1973.

Fredricks, R. W., G. M. Crook, C. F. Kennel, I. M. Green, F. L. Scarf, P. J. Coleman, Jr., and C. T. Russell, OGO 5 observations of electrostatic turbulence in bow shock magnetic structures, J. Geophys. Res., 75, 3751, 1970.

Fried, B. D., and R. W. Gould, Longitudinal ion oscillations in a hot plasma, Phys. Fluids, 4, 139, 1961.

Greenstadt, E. W., Structure of the terrestrial bow shock, Solar Wind Three, Proc. Third Solar Wind Conference, Asilomar, Ed. C. T. Russell, Institute of Geophysics & Planetary Physics, UCLA, 440, 1974.

Greenstadt, E. W., C. T. Russell, F. L. Scarf, V. Formisano and M. Neugebauer, Structure of the quasi-perpendicular laminar bow shock, J. Geophys. Res., 80, 502, 1975.

Manheimer, W. M., and J. P. Boris, Self-consistent theory of a collisionless, resistive shock, Phys. Rev. Lett's., 28, 659, 1972.

Montgomery, M. D., J. R. Asbridge, and S. J. Bame, Vela 4 plasma observations near the earth's bow shock, J. Geophys. Res., 75, 1217, 1970.

Neugebauer, M., C. T. Russell, and J. V. Olson, Correlated observations of electrons and magnetic fields at the earth's bow shock, J. Geophys. Res., 76, 4366, 1971.

Case	PARAMETERS MEASURED OR ASSUMED						CALCULATED PARAMETERS				CALCULATED SHOCK THICKNESSES			
	Θ_{BU}	$B_1(\gamma)$	$B_2(\gamma)$	T_{e1} °K	T_{i1} °K	$n_1(cm^{-3})$	β_1	$n_2(cm^{-3})$	T_{e2} °K	$n^{(20)}(cm^{-3})$	L_{S1} km	L_{S2} (km)	$L_S^{(20)}$ (km)	[illegible] L
[illegible] Case 1	62°	13.5	33	1.5×10^5	1.4×10^4	2.0	.07	4.5	1.1×10^6	2.3	430	370	720	[illegible]
Case 2	73°-80°	13	30	1.5×10^5	2×10^4	2.5	.09	5.8	1.2×10^6	3.3	170	210	370	[illegible]
Case 3	73°-79°	12.5	32	1.5×10^5	5.8×10^4	2.5	0.11	6.5	1.6×10^6	5.6	50	120	140	[illegible]
Case 4	84°-88°	7.5	20	1.5×10^5	1.9×10^4	2.0	0.1	6.3	1.7×10^6	2.5	170	170	320	[illegible]
[illegible] (typical values)	>60°	6	18	1×10^5	5×10^4	10	1.45	30	8.4×10^5	—	6.7	9.0	—	[illegible]

[illegible]

NOTES

1. n_2 CALCULATED FROM $n_2 = (B_2/B_1)\,n_1$ except in first case where $\Theta_{BU} < 75°$, AT LOW M_A.

2. n_1 CHOSEN AT MAXIMUM OF RANGE GIVEN IN FIRST 4 CASES, FOR BEST AGREEMENT WITH CONSERVATION LAWS.

3. T_{e2} CALCULATED FROM UPSTREAM T'S AND CONSERVATION LAWS, ASSUMING ALL IRREVERSIBLE HEATING GOES TO ELECTRONS, FOR FIRST 4 (SUBCRITICAL) CASES. FOR LAST CASE, T_{e2} TAKEN TO BE COMPARABLE WITH MEASUREMENTS OF MONTGOMERY, et al., UNDER SIMILAR CONDITIONS.

4. IN COMPUTING L_S, T_i ASSUMED = T_{i1} SINCE THE COMPRESSION WILL SPREAD THE ION VELOCITIES [illegible], THE SHOCK [illegible], ⊥ TO THE [illegible].

5. $n^{(20)}$ AND $L^{(20)}$ [illegible] FOR CONDITIONS AT WHICH T REACHES 20 × T_{i1}, THE [illegible] MINIMUM L_S. T_e does not reach 20 T_{i1} in the last case.

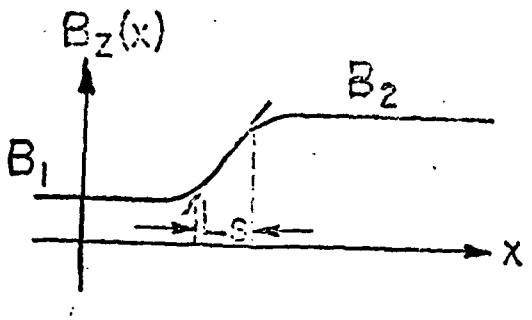

Figure 1. Model Magnetic Gradient

STABILITY BOUNDARY FOR CURRENT-DRIVEN ELECTROSTATIC WAVES

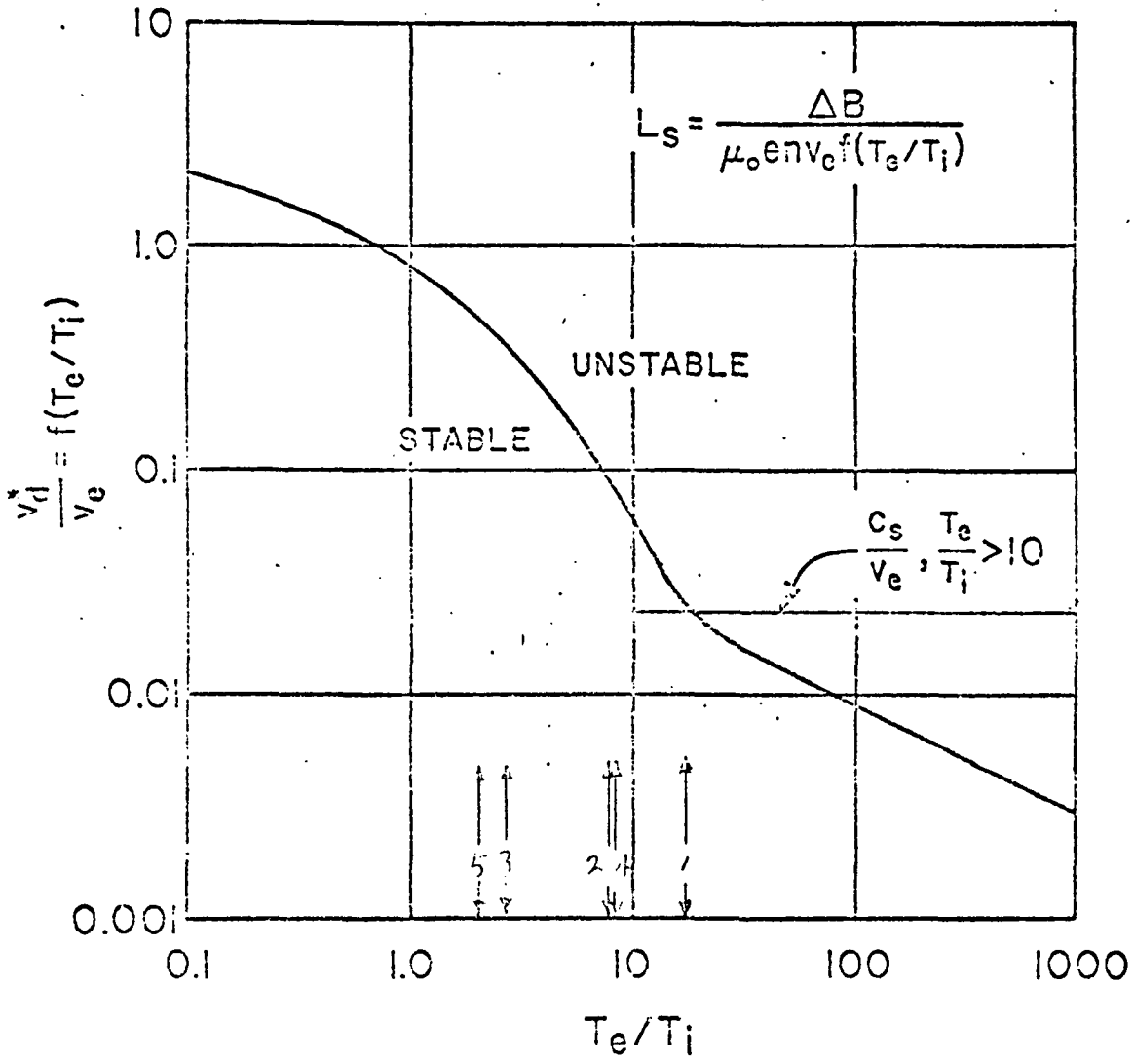

Figure 2 Stability boundary as computed by Fried and Gould (Phys. Fluids 4, 139 (1961)). Here $C_s^2 = kT_e/M_i$ is ion-acoustic speed, for $T_e/T_i > 10$.

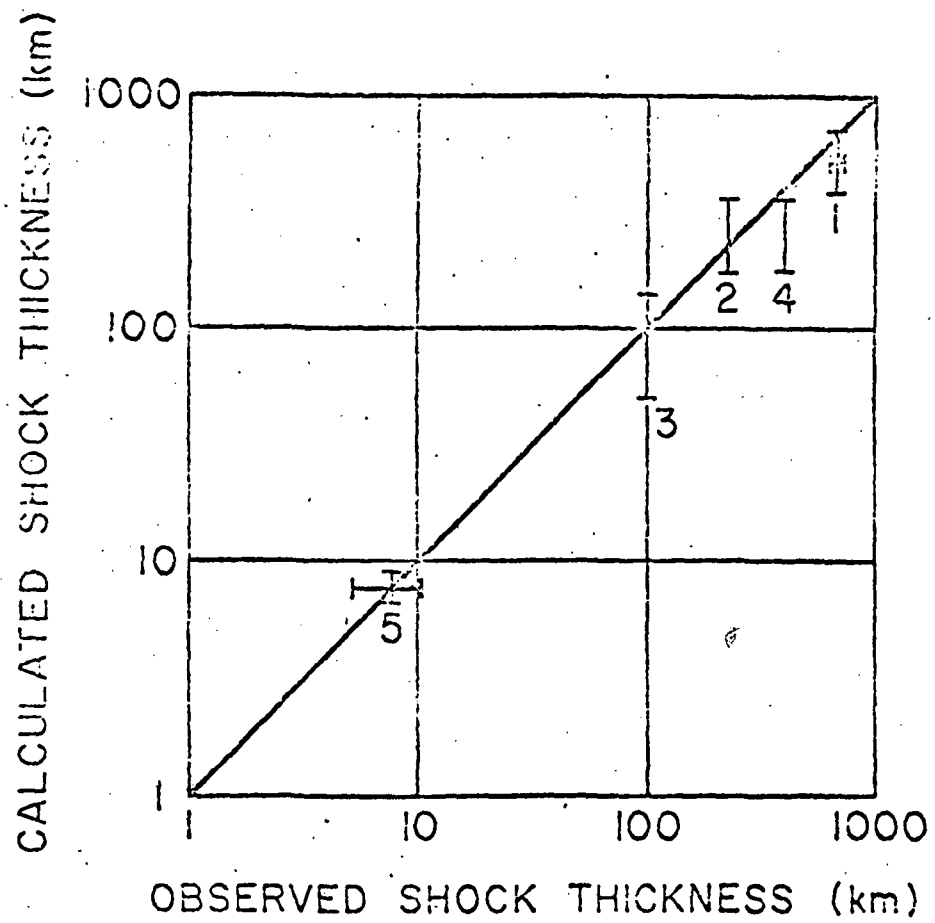

Figure 3 Comparison of measured and calculated shock thicknesses. Cases 1-4 are cases 1-4 of Greenstadt et al (J. Geophys. Res. 80, 502 (1975)). Case 5 is typical of data of Fredricks et al [J. Geophys. Res. 75, 3751 (1970)].